land

MDPI

Article

Spatial–Temporal Variation and Driving Forces of Carbon Storage at the County Scale in China Based on a Gray Multi-Objective Optimization-Patch-Level Land Use Simulation-Integrated Valuation of Ecosystem Services and Tradeoffs-Optimal Parameter-Based Geographical Detector Model: Taking the Daiyun Mountain's Rim as an Example

Gui Chen [1], Qingxia Peng [1,2], Qiaohong Fan [1], Wenxiong Lin [1,2,*] and Kai Su [1,2,3,*]

[1] Institute of Agroecology, College of Digital Economy, Fujian Agriculture and Forestry University, Fuzhou 350002, China; cg975787912@fafu.edu.cn (G.C.); fan123456@fafu.edu.cn (Q.F.)
[2] Fujian Provincial Key Laboratory of Agroecological Processing and Safety Monitoring, Fuzhou 350002, China
[3] Ecological Civilization Research Center, Fujian Agriculture and Forestry University, Fuzhou 350002, China
* Correspondence: lwx@fafu.edu.cn (W.L.); fjsk1311@fafu.edu.cn (K.S.)

Abstract: Exploring and predicting the spatiotemporal evolution characteristics and driving forces of carbon storage in typical mountain forest ecosystems under land-use changes is crucial for curbing the effects of climate change and fostering sustainable, eco-friendly growth. The existing literature provides important references for our related studies but further expansion and improvements are needed in some aspects. This study first proposed an integrated framework comprising gray multi-objective optimization (GMOP), Integrated Valuation of Ecosystem Services and Tradeoffs (InVEST), the Patch-level Land Use Simulation Model (PLUS), and optimal parameter-based geographical detector (OPGD) models to further expand and improve on existing research. Then, the integrated model was used to analyze the spatial–temporal variation in land-use pattern and carbon storage at the county scale in China's Daiyun Mountain's Rim under four scenarios in 2032, and analyze the driving force of spatial differentiation of carbon storage. The results indicated that (1) land-use change primarily involves the mutual transfer among forest, cultivated, and construction land, with approximately 7.2% of the land-use type area undergoing a transition; (2) in 2032, the natural development scenario projects a significant reduction in forest land and an expansion of cultivated, shrub, and construction lands. Conversely, the economic priority, ecological priority, and economic–ecological coordinated scenarios all anticipate a decline in cultivated land area; (3) in 2032, the natural development scenario will see a 2.8 Tg drop in carbon stock compared to 2022. In contrast, the economic priority, ecological priority, and economic–ecological coordinated scenarios are expected to increase carbon storage by 0.29 Tg, 2.62 Tg, and 1.65 Tg, respectively; (4) the spatial differentiation of carbon storage is jointly influenced by various factors, with the annual mean temperature, night light index, elevation, slope, and population density being the key influencing factors. In addition, the influence of natural factors on carbon storage is diminishing, whereas the impact of socioeconomic factors is on the rise. This study deepened, to a certain extent, the research on spatiotemporal dynamics simulation of carbon storage and its driving mechanisms under land-use changes in mountainous forest ecosystems. The results can serve to provide scientific support for carbon balance management and climate adaptation strategies at the county scale while also offering case studies that can inform similar regions around the world. However, several limitations remain, as follows: the singularity of carbon density data, and the research scope being confined to small-scale mountainous

Academic Editors: Xuechao Wang, Weize Song and Yingjie Li

Received: 19 November 2024
Revised: 18 December 2024
Accepted: 23 December 2024
Published: 25 December 2024

Citation: Chen, G.; Peng, Q.; Fan, Q.; Lin, W.; Su, K. Spatial-Temporal Variation and Driving Forces of Carbon Storage at the County Scale in China Based on a Gray Multi-Objective Optimization-Patch-Level Land Use Simulation-Integrated Valuation of Ecosystem Services and Tradeoffs-Optimal Parameter-Based Geographical Detector Model: Taking the Daiyun Mountain's Rim as an Example. *Land* **2025**, *14*, 14. https://doi.org/10.3390/land14010014

forest ecosystems. Future studies could consider collecting continuous annual soil carbon density data and employing land-use simulation models (such as PLUS or CLUMondo) appropriate to the study area's dimensions.

Keywords: land-use change; GMOP-PLUS-OPGD; carbon storage; GeoDetector; multi-scenario simulation

1. Introduction

Anthropogenic climate change has triggered oceanic acidification and an increased frequency of extreme weather events, prompting a basic international consensus on capturing and sequestering carbon emissions [1]. Terrestrial ecosystems have a significant carbon sink function, annually absorbing approximately 28% of anthropogenic CO_2 emissions [2], sequestering them as organic matter, thereby effectively reducing atmospheric CO_2 concentrations [3,4]. Land-use change has emerged as a primary driving force influencing terrestrial ecosystem services, spatial patterns, and the overall provision of carbon storage [5–8]. Shifts in land-use patterns affect regional carbon stocks by altering surface material cycles, energy flows, and the potential for soils and vegetation to sequester carbon [9,10]. Some studies have indicated that approximately 19% of cumulative global CO_2 emissions from 1850 to 2019 were attributed to land-use change activities [11]. Furthermore, research has shown that natural ecosystems such as forests and grasslands in the Northern Hemisphere's mid-to-high latitudes, particularly forest ecosystems, possess a formidable carbon sequestration capacity, absorbing 2–3 billion tons of carbon dioxide annually, rendering them a major spatial carrier of carbon sink on land [12,13]. Major forest nations, notably China, Brazil, Canada, the Democratic Republic of Congo, Russia, and the United States, play a pivotal role in global carbon cycling, accounting for a substantial 51% of global emissions, 56% of total carbon sequestration, and 60% of net carbon flux [14]. To address climate change's impact on human well-being and sustainable socioeconomic development, The Intergovernmental Panel on Climate Change (IPCC) has established comprehensive guidelines for anthropogenic greenhouse gas emissions and removals [15,16], enabling governments worldwide to optimize land resource management and enhance carbon sink capacity. In 2021, representatives from 145 nations collectively endorsed the *Glasgow Leaders' Declaration on Forests and Land Use*. This landmark declaration articulates a shared commitment among signatories to safeguard and expedite the restoration of forests and other terrestrial ecosystems, with a pledged deadline of 2030 to halt and reverse forest loss and land degradation [17]. Against this backdrop, China introduced its "dual carbon" goals in 2020 (peaking carbon emissions by 2030 and achieving carbon neutrality by 2060) with specific objectives such as increasing national forest land coverage to approximately 25% and stock volume to 19 billion m^3 by 2030, and surpassing non-fossil energy usage above 80% by 2060 [18]. These outlined actions demonstrate the critical need for continually strengthening carbon sink capacity in order to achieve China's "dual carbon" goals. China's "dual carbon" goal will inject vital impetus into the global climate governance process [19]. Consequently, exploring the effect of land-use changes on carbon sequestration in China's terrestrial regional ecosystems, probing the driving factors behind ecosystem carbon stocks, and exploring the optimization of spatial patterns to enhance terrestrial ecosystem carbon sequestration is of paramount importance for achieving the "dual carbon" targets and addressing global climate change [20].

Currently, the approach for assessing carbon stocks in terrestrial ecosystems in the literature encompasses field surveys, remote-sensing inversion, and model simulations [21]. Field surveys directly and accurately measure carbon stocks in small-scale ecosystems but

entail substantial workloads and time consumption [22]. Remote-sensing inversion is solely suitable for analyzing specific ecosystems at a macro scale [23,24]. The model simulation method is an effective approach for estimating the dynamic changes in ecosystem carbon storage at multiple scales. Simulations offer ease of operation and faster speeds while enabling spatiotemporal quantitative analyses and intuitive visualization of carbon stocks across different scales [25]. The InVEST model stands out among various models due to its strong versatility, low demand, and other features. In particular, its carbon storage module provides more accurate estimations compared to other models [26], making it widely utilized [27,28]. A growing quantity of studies are combining the InVEST model with Flow-direction-based Landscape Urban Simulation (FLUS) [29], Cellular Automata–Markov (CA–Markov) [30], Conversion of Land Use and its Effects at Small region extent (CLUE-s) [31], and CLUMondo [32] models to forecast future carbon stocks and land-use spatial distribution under multiple scenarios. Additionally, Lyu et al. [33] have demonstrated that coupled models can effectively improve simulation accuracy.

From the current research progress of domestic and international scholars, the academic community has achieved fruitful results in land-use change, carbon stock estimation, and multi-scenario prediction. However, traditional commonly used models are hard to employ to flexibly forecast changes at the patch level in a range of land-use types and lack in analyzing the driving factors and influence mechanisms. Overall, the existing literature provides important references for our related studies but further expansion and improvements are needed in the following aspects: (1) Carbon density data are often derived from previous studies, which may differ significantly from field measurements [25,34–36]. Scholars tend to analyze carbon stock changes at the horizontal scale, overlooking the spatial heterogeneity and the influence of multi-dimensional environmental gradients in complex terrain regions. (2) The PLUS model can precisely simulate non-linear relationship changes in land-use change processes [37]. It outperforms models such as FLUS, CA–Markov, and CLUE-s in terms of simulation accuracy, cell-scale changes, and landscape pattern similarity [38]. The PLUS model has a high degree of coupling with the InVEST model and is currently an effective means for land-use change scenario prediction [39]. Consequently, numerous studies have coupled the InVEST model with the PLUS model, not only assessing ecosystem service functions but also predicting various future land-use scenarios and enabling the evaluation of ecosystem service capabilities under future multi-scenarios [28,32,40]. However, some scholars have pointed out that the PLUS model cannot effectively simulate when it involves climate factors, natural factors, and dynamic socioeconomic policies [41]. (3) Land-use scenario simulation is an important method for achieving optimal land-use allocation [42]. Structural prediction in land-use scenario modeling mainly includes the Markov model [43], System Dynamics (SD) model [44], and GMOP model [45]. Among these, the GMOP model can handle uncertainties in objective functions and constraint conditions, integrating multi-objective linear programming and grey prediction theory, which can better reflect dynamic evolution characteristics [46]. However, rapid urbanization has produced complex land-use and carbon storage distribution patterns at multiple scales. In addition to socioeconomic and natural factors, specific policies also have an impact on land-use change [47]. The Markov chain built into the PLUS model used in the existing study of carbon reserves cannot satisfy the prediction and simulation of non-linear quantities for ecosystem service types like carbon storage, making it difficult to respond to environmental protection policy demands and objectively coordinate the research area's ecological and economic benefits to optimize land-use structure [48]. Therefore, coupling the GMOP model with the PLUS model not only leverages the unique advantages of both models in structural optimization, scenario setting, and spatial allocation but also effectively avoids the uncertainties and limitations of the PLUS model. (4) The existing

literature trends toward analyzing the driving mechanisms of carbon stocks solely from the land-use change perspective, lacking in-depth research on the impact of natural and socioeconomic factors [49]. Geodetector is a commonly used method for investigating driving factors [50]. However, most scholars [51,52] discretize continuous independent variables based on subjective experience but the parameters derived from this classification approach may not necessarily be the optimal parameter. Song et al. [53] proposed an optimum parameter-based geo-detector (OPGD) that can identify the optimal combination of spatial scale parameters and spatial data discretization classification methods as well as identify the driving factors of phenomena and their spatial heterogeneity distribution characteristics, largely compensating for the deficiencies of traditional geographical detectors. Given this, regional soil data can be used to calculate soil carbon density, and the prediction results of the GMOP model can be applied to the structural prediction step of the InVEST-PLUS model. This model's combined approach not only preserves the unique functions of each model but also effectively compensates for the single model's deficiencies, thereby enabling reasonable and objective predictions of carbon storage changes under future scenarios. Additionally, adopting the OPGD model will address the deficiencies of traditional carbon storage research in exploring driving mechanisms and provide a reasonable and scientific basis for making decisions in order to optimize land spatial patterns and enhance regional carbon storage.

The hilly regions of Southern China are an important carbon storage area in the country [54]. To promote economic growth through the utilization of ecological assets, a green economic industry alliance was established in 2023 by the six counties of the Daiyun Mountain's Rim in Southern China, namely Dehua, Yongchun, Yongtai, Datian, Youxi, and Xianyou. This region is characterized by its abundant biodiversity and extensive river networks within its mountainous forest ecosystems [55], possessing invaluable ecological significance. As the basic units of China's national economy, counties play an irreplaceable role in optimizing the economic structure, promoting social stability and eco-environmental governance. However, China's prioritization of urbanization at the county level has compressed ecological spaces, leading to an increase in CO_2 emissions and a decline in ecological quality and carbon stock across numerous regions in the southern hilly areas [56,57]. Scientifically assessing and enhancing the ecological resource endowment of this region—particularly the carbon sequestration potential of various land-use types in terrestrial ecosystems—while optimizing the spatial pattern of land use to unlock development potential has become an urgent realistic issue. This issue not only pertains to the sustainable development of regional green industries but is also a crucial component in responding to global climate change and meeting the "dual carbon" goals. Accordingly, this study proposed an integrated framework comprising GMOP, InVEST, PLUS, and OPGD models, optimizing the land-use allocation from the dual perspectives of ecological preservation and economic growth, simulating and projecting future land-use patterns across multiple scenarios over the next decade, i.e., 2032. Through investigating the spatiotemporal evolution of carbon stocks and land-use types and detecting drivers of carbon storages from an optimal parameter perspective to rationally optimize the national spatial pattern, this approach is not only crucial for achieving the "dual carbon" goals and supporting the sustainable development of green industries in the Daiyun Mountain's Rim but will also provide a significant reference for seeking a balance between ecological resource conservation and economic growth in other similar southern hilly areas of China, contributing to the global effort in response to climate change.

2. Materials and Methods

2.1. Overview of the Study Area

The Daiyun Mountain's Rim (25°21′–26°10′ N, 118°11′–118°55′ E) is located in Fujian Province, a hilly region in Southern China (Figure 1) and encompasses six counties: Dehua, Yongchun, Yongtai, Datian, Youxi, and Xianyou. The total area is approximately 13,424 km^2. The region has an average altitude of 589 m and experiences a mean annual temperature range of 16.0–27.0 °C with an average annual precipitation of 1400–2300 mm. The region falls within the subtropical monsoon climate zone, which results in mild weather with distinct seasons. The terrain exhibits significant fluctuations characterized by low- to mid-mountain features. Notably, the Daiyun Mountain Nature Reserve in Dehua County is often referred to as the "spine of central Fujian" due to its impressive forest land coverage rate of 93.4% [55]. In 2022, Fujian Province released the "*Implementation Opinions on Comprehensively, Accurately, and Fully Implementing New Development Concepts to Deliver on Carbon Peaking and Carbon Neutrality Goals*" document that outlines the target of increasing the forest land coverage rate by 0.19% and achieving a forest land stock volume of 800 million m^3 by 2030 compared to the levels of 2020. It also emphasizes reinforcing provincial territorial spatial planning and strictly protecting natural ecosystems such as wetlands, forests, grasslands, and soils that are significant for carbon fixation. These measures support the goals of carbon peaking and carbon neutrality. Notably, there is a strong focus on implementing ecological protection and restoration projects aimed at enhancing the carbon sink capacities of Mount Dayun's forest ecosystems.

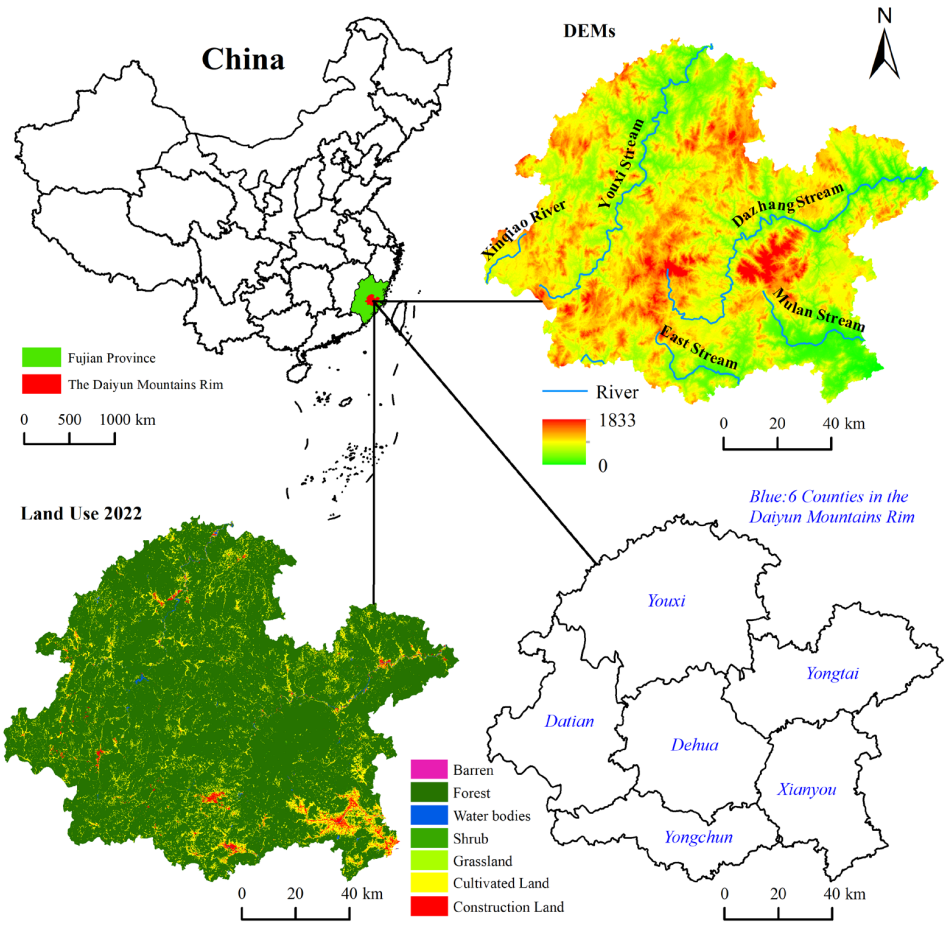

Figure 1. Overview of the Daiyun Mountain's Rim.

2.2. Data Sources

This study's data primarily include 7 periods (1992, 1997, 2002, 2007, 2012, 2017, and 2022) of land-use data, natural factor data, socioeconomic data, and accessibility data for the Daiyun Mountain's Rim (Table 1). According to the purpose of this research and the current status of the Daiyun Mountain's Rim, land-use types are categorized into 7 types: cultivated land, forest, shrub, grassland, water bodies, barren, and construction land.

Table 1. Main information and sources of data.

Dimension	Dataset Name	Spatial Resolution	Data Source
Land use	7 periods of land-use data	30 m	The 30-m annual land cover datasets and the dynamics in China from 1985 to 2022 (https://zenodo.org/records/8176941, accessed on 2 July 2024)
Natural factors	Soil data		FOA (www.fao.org, accessed on 3 July 2024)
	Digital elevation models (DEMs) (X1)	30 m	Geospatial data cloud (https://www.gscloud.cn/, accessed on 3 July 2024)
	Slope (X2)	30 m	
	Aspect (X3)	30 m	
	Annual precipitation (X4)	1000 m	Chinese Academy of Sciences (https://www.resdc.cn, accessed on 5 July 2024)
	Average annual temperature (X5)	1000 m	
	Soil type (X6)	1000 m	
	Soil erosion intensity (X7)	1000 m	
	Net Primary Production (NPP) (X8)	500 m	NASA (https://www.earthdata.nasa.gov/, accessed on 5 July 2024)
Socioeconomic factors	Gross domestic product (GDP) (X9)	1000 m	Chinese Academy of Sciences (https://www.resdc.cn, accessed on 8 July 2024)
	Population density (X10)	1000 m	
	Night light index (X11)	500 m	
Locational factors	Distance to highway (X12)	500 m	National catalog service for geographic information (https://www.webmap.cn, accessed on 8 July 2024)
	Distance to primary roads (X13)	500 m	
	Distance to secondary roads (X14)	500 m	
	Distance to tertiary roads (X15)	500 m	
	Distance to class quaternary roads (X16)	500 m	
	Distance to water (X17)	500 m	
	Distance to county and township government offices (X18)	500 m	

2.3. GMOP Model

The GMOP model integrates the GM (1, 1) and Multi-Objective Optimization (MOP) models. Specifically, it employs GM (1, 1) to predict value coefficients of the economic and ecologic factors for various forms of land use in 2032, incorporating these predictions into the objective function of the MOP model. This model first defines decision variables, objec-

tive functions, and constraints for different scenarios, optimizing the structural allocation of diverse land-use types within the region, thereby solving the regional land-use demand.

2.3.1. Land-Use Value Coefficient

This study—according to the ecological value coefficient calculation approach proposed by Xing et al. [58]—utilizes annual crop yield, cultivated area, and average annual price data for major crops (due to data availability constraints for some counties, corresponding data at the prefecture-level city are used), coupled with Xie et al.'s [59] research findings to calculate the ecological value coefficients for various land-use types within the research area for various years in the past. Furthermore, following the approach of Wang et al. [60], the economic value coefficients of cultivated land, forest, shrub, grassland, water bodies, and constructed land are estimated using annual output values per unit area of agriculture, forestry, livestock, fisheries, and secondary and tertiary industries in each of the six counties from 2013 to 2022. Finally, based on the economic and ecological value coefficients of seven land types in the Daiyun Mountain's Rim, the GM (1, 1) model is employed to predict the economic and ecological value coefficients of seven land-use types in 2032 (Table 2).

Table 2. Coefficients of economic value and ecological value of land-use types in the Daiyun Mountain's Rim (10^4 CNY/hm^2).

Land-Use Type	Cultivated Land	Forest Land	Shrub	Grassland	Water Bodies	Barren	Construction Land
Economic value coefficients	18.35	0.93	0.93	5623.54	38.06	0	2862.44
Ecological value coefficients	4.38	26	17.14	22.17	141.44	0.23	0

2.3.2. Objective Function Construction

Based on the land-use structure and socioeconomic development trends in the Daiyun Mountain's Rim, this study establishes four scenarios: natural development scenario (ND), economic priority development scenario (ED), ecological priority development scenario (EP), and coordinated economic–ecological development scenario (CD). These scenarios are employed to optimize and analyze the land-use structure.

The economic priority development scenario aims to an seek optimal allocation scheme for maximizing economic returns from various land types within the Daiyun Mountain's Rim.

$$f_1(x) = \sum_{1}^{7} ec_i \times x_i \tag{1}$$

The ecological priority development scenario aims to seek the optimal allocation scheme for maximizing ecological returns from various land types within the Daiyun Mountain's Rim.

$$f_2(x) = \sum_{1}^{7} esv_i \times x_i \tag{2}$$

The coordinated economic–ecological development scenario aims to seek a new harmonious balance point between economic growth and ecological preservation within the Daiyun Mountain's Rim.

$$f_3(x) = \max\{f_1(x), f_2(x)\} \tag{3}$$

In Equations (1) and (2), ec_i and esv_i represent the economic value coefficient (10^4 CNY/hm^2) and ecological value coefficient (10^4 CNY/hm^2) per unit area of i land-use type, respectively.

2.3.3. Constraint Condition

Given the constraints imposed on land-use structure by real conditions such as socioeconomic policies, in order to thoroughly consider the demands of ecological conservation and socioeconomic growth, the constraints in this study are established based on existing research, policy plans, and spatial realities (Table 3). By incorporating the objective functions and constraints under the three scenarios into LINGO 18.0 for solving, we can obtain the land-use demand projections in 2032 under the three scenarios.

Table 3. Different land-use type constraints (hm^2).

Constraint type	Formulas	Formula Interpretation
Total area	$\sum_{i=1}^{7} x_i = 1335800.34$	The total area of all land-use types should remain constant.
Cultivated land demand	$x_1 \geq 99829.72$	According to the Fujian Provincial Land-use Master Plan (2006–2020), the lower limit of presumed cultivated land area
Forest land demand	$x_2 \geq 1178438.04$	Following the "Implementation Opinions" issued by the Fujian Provincial Party Committee and Provincial Government, a 0.19% increase in forest land area by 2020 is set as the lower bound for forest land area in 2032.
Shrub demand	$x_3 \leq 136.8$	As grassland area has exhibited a declining trend over the past decade, the grassland area in 2022 is designated as the upper limit.
Grassland demand	$x_4 \leq 280.89$	Grassland areas have shown a downward trend over the past 10 years; therefore, 2022 was used as the upper limit for grassland areas.
Water bodies' demand	$x_5 \geq 4381.02$	As this region serves headwater bodies for numerous rivers, and the water body area has exhibited a decreasing trend over the past 10 years, the water body area in 2022 is set as the lower limit.
Construction land demand	$x_7 \geq 17105.76$	Construction land is generally more stable and less susceptible to conversion to other land-use types; therefore, the 2022 built-up land area is used as a lower bound.
Barren land demand	$4.14 \leq x_6 \leq 13.68$	The barren land area has surged over the past 10 years. Under various scenarios, barren land requires rational development and utilization, aiming to restore it to the 2012 level. Therefore, the upper limit for barren land area is set at the 2022 level, while the lower limit is set at the 2012 level.
Model accuracy	$0.8y_i \leq x_i \leq 1.2y_i$	For land-use types with undetermined upper and lower limits across scenarios, the baseline is set as the projection from the Markov model, with a fluctuation range of 20%.
Variables non-negative constraints	$x_i, y_i \geq 0, i = 1, 2 \ldots, 7$	The decision variables must be non-negative, with x_i and y_i representing the areas of cultivated, forest, shrub, grassland, water bodies, barren land, and construction land under the optimized scenarios and natural development scenario, respectively.

2.4. PLUS Simulating Future Multi-Scenario Land-Use Patterns

In this study, the PLUS model was employed to simulate and analyze multi-scenario land use for the Daiyun Mountain's Rim in 2032. First, the data from 2012 and 2022 land use acted as the foundation for extracting the expansion portion. Secondly, 18 driving factors of natural, socioeconomic, and accessibility factors were selected (Table 1), and the random forest algorithm in the land expansion analysis strategy (LEAS) module was utilized to obtain the potential transition probabilities and development trends of land-use types in the area; this took 2012 land-use data as the baseline map and combined domain-specific weights and land-use demand obtained from the GMOP model as parameters in the CA based on the multi-type random patch seeds (CARS) module, enabling the simulation to obtain a land-use raster map in 2022.

2.4.1. LEAS Module

The LEAS transforms the extraction of land-use transition rules between two temporal datasets into a binary classification problem by analyzing paired land-use data. Through the Random Forest Classification (RFC) algorithm, it uncovers the patterns of land-use transitions and calculates the growth probability for each land-use type [37], as expressed in the following formula:

$$P_{i,k(X)}^{d} = \frac{\sum_{n=1}^{M} I[h_n(X) = d]}{M} \tag{4}$$

where $P_{i,k(X)}^{d}$ denotes the growth probability of spatial unit i transitioning to land-use type k under condition d (0 or 1); X represents a vector comprising multiple driving factors; $h_n(X)$ signifies the predicted land-use type by the *n-th* decision tree for vector X; I serves as the indicator function of the decision tree; M represents the total number of decision trees; and $d = 1$ indicates the transformation from other land-use types to type k, while $d = 0$ indicates that no conversion to type k occurs.

2.4.2. CARS Module

Based on the growth probabilities (land expansion maps) calculated by the LEAS module, the CARS module employs a Cellular Automata model with multi-class random seed generation [37] to identify and extract the driving forces behind land expansion and landscape transformation, thereby predicting and determining the spatial distribution of future land-use patterns. The formula for calculating the overall probability of land-use type k is expressed as follows:

$$OP_{i,k}^{d=1,t} = P_{i,k}^{d=1} \times \Omega_{i,k}^{t} \times D_{k}^{t} \tag{5}$$

where $OP_{i,k}^{d=1,t}$ denotes the growth probability of spatial unit i transitioning to land-use type k at time t; $P_{i,k}^{d=1}$ represents the growth probability of spatial unit i converting to land-use type k; $\Omega_{i,k}^{t}$ signifies the neighborhood effect of land-use type k within the vicinity of unit i at time t; D_{k}^{t} is an adaptive driving coefficient that reflects the impact of future demand for land-use type k during the *t-th* iteration.

$$\Omega_{i,k}^{t} = \frac{con(c_i^{t-1} = k)}{n \times n - 1} \times w_k \tag{6}$$

where $con(c_i^{t-1} = k)$ represents the total number of grid cells occupied by land-use type k within an $n \times n$ cellular matrix during the final iteration; w_k denotes the neighborhood weight coefficient for land-use type k, with a default value of 1.

$$D_k^t = \begin{cases} D_k^{t-1} & \left(\left|G_k^{t-1}\right| \leq \left|G_k^{t-2}\right|\right) \\ D_k^{t-1} \times \frac{G_k^{t-2}}{G_k^{t-1}} & (0 > G_k^{t-2} > G_k^{t-1}) \\ D_k^{t-1} \frac{G_k^{t-1}}{G_k^{t-2}} & G_k^{t-1} > G_k^{t-2} > 0 \end{cases} \tag{7}$$

where G_k^{t-1} and G_k^{t-2} represent the differences between the actual quantity and demand of land-use type k during iterations $t-1$ and $t-2$, respectively.

The model employs a competitive process threshold descent mechanism to simulate the natural growth of various land types during patch evolution, expressed by the following formula:

$$OP_{i,k}^{d=1,t} = \begin{cases} P_{i,k}^{d=1} \times (r \times \mu_k) \times D_k^t & (\Omega_{i,k}^t = 0, r < P_{i,k}^{d=1}) \\ P_{i,k}^{d=1} \times \Omega_{i,k}^t \times D_k^t & others \end{cases} \tag{8}$$

where r represents a random value ranging between 0 and 1; μ_k denotes the threshold for generating new patches of the *k-th* land-use category.

When a novel land-use classification emerges victorious through the competitive mechanism, the model employs a patch generation threshold decay coefficient τ to evaluate the candidate land-use type c, selected via roulette wheel selection, as expressed in the following equation:

$$\text{If} \sum_{k=1}^{N} \left|G_c^{t-1}\right| - \sum_{k=1}^{N} \left|G_c^t\right| < Step \quad Then, l = l + 1 \tag{9}$$

$$\begin{cases} Change & P_{i,c}^{d=1} > \tau \quad and \quad TM_{k,c} = 1 \\ No\ change & P_{i,c}^{d=1} \leq \tau \quad or \quad TM_{k,c} = 0 \end{cases} \qquad \tau = \delta^l \times r_1 \tag{10}$$

where N represents the total number of land-use types; *Step* denotes the required interval length in the PLUS model for land-use demands. The coefficient δ, which ranges between 0 and 1, serves as the decay parameter for threshold τ. The variable r_1 represents a random value following a normal distribution with a mean of 1; and l signifies the number of decay steps. $TM_{k,c}$ constitutes the transition matrix, which defines whether land-use type k may be converted to type c, with values of 0 or 1 indicating permitted and restricted transitions, respectively.

2.4.3. PLUS Model Accuracy

The PLUS model's overall accuracy was 0.9386, with Kappa and FOM coefficients of 0.7159 and 0.1558, respectively, indicating a high simulation accuracy of PLUS, capable of effectively modeling land-use changes in the study region. Finally, using 2022 land-use data as the baseline and incorporating the land-use transition matrix and land demand parameters, the land-use patterns were simulated for 2032 under multi-scenarios.

2.5. InVEST Model of Carbon Storage Assessment

InVEST is a suite of integrated ecosystem service assessment models that employ production function approaches to establish linkages between ecosystem structure and function changes and the flow and worth of ecosystem service provisioning. It enables the quantitative analysis and spatial expression of diverse ecosystem services [61]. A terrestrial ecosystem sub-model of the InVEST "carbon storage and sequestration" adopts a land-use

type-based approach to estimate terrestrial ecosystems' carbon stocks, serving as an effective contemporary method for appraising carbon storage in terrestrial ecosystems [25,62].

The "carbon storage and sequestration" module was employed in this study to calculate carbon stocks at the pixel scale within the study area based on the aboveground carbon pool (C_{above}), belowground carbon pool (C_{below}), soil carbon pool (C_{soil}), and dead organic matter/dead wood carbon pool (C_{dead}) combined with the area of each land-use type from 1992 to 2022. This approach is convenient, efficient, and yields intuitive outcomes. Previous studies have demonstrated that incorporating this module into the InVEST model effectively captures spatiotemporal distribution patterns of regional terrestrial carbon sinks [63]. The specific computational formulas are as follows:

$$Ci\text{-}total = Ci\text{-}above + Ci\text{-}below + Ci\text{-}soil + Ci\text{-}dead \quad (11)$$

$$Ctotal = \sum_{i}^{m} CiSi \quad (12)$$

In Equation (11), i represents land-use type; $C_{i\text{-}total}$ represents total carbon density ($t \cdot hm^{-2}$) of land-use type i; $C_{i\text{-}above}$, $C_{i\text{-}below}$, $C_{i\text{-}soil}$, and $C_{i\text{-}dead}$ refer to carbon density ($t \cdot hm^{-2}$) of aboveground biomass, belowground biomass, soil, and dead wood, respectively, for land-use type i.

In Equation (12), C_{total} refers to the total terrestrial ecosystem carbon stocks (t); S_i represents the total area (hm^2) of land-use type i; m denotes the number of land-use types—m is 7 in this study.

2.6. Carbon Density Calculation

The soil property values necessary for computing varying soil carbon densities across the study area were obtained from the Harmonized World Soil Database. Equation (13) outlines the formula used to calculate topsoil carbon density [64].

$$C_{soil} = TOC \times y \times H \times 10^{-1} \quad (13)$$

where C_{soil} represents soil carbon density ($t \cdot hm^{-2}$); TOC refers to organic carbon content ($t \cdot t^{-1}$); y denotes the mean soil bulk density ($kg \cdot m^{-3}$); and H signifies the mean depth (m) of the topsoil layer for specific soil types. The data on aboveground and belowground vegetation carbon density, as well as dead organic matter carbon density, were obtained from the National Ecological Science Data Center (http://www.cnern.org.cn/, accessed on 10 July 2024) and assigned values according to Han et al. [65]. This facilitated determining four parameter components—aboveground carbon density, belowground carbon density, soil carbon density, and dead organic matter carbon density—across the study area, as presented in Table 4.

Table 4. Carbon intensity of different land-use types in the Daiyun Mountain's Rim.

Land-Use Type	C_{above}/t·hm^{-2}	C_{below}/t·hm^{-2}	C_{soil}/t·hm^{-2}	C_{dead}/t·hm^{-2}
Forest land	65.87	12.25	51.05	2.11
Cultivated land	3.91	1.53	50.37	0
Shrub	5.41	1.79	53.45	1.01
Grassland	1.63	4.11	53.56	1.81
Water bodies	0.00	0.00	45.34	0
Barren	0.67	9.37	45.84	0
Construction land	0.93	0.25	45.23	0

2.7. The Topographic Position Index Calculation

Digital elevation models (DEMs) have proven to be essential tools in extracting and characterizing both macroscopic and microscopic terrain attributes in various studies. Terrain variables such as slope, aspect, and surface ruggedness collectively exert significant influence on geomorphic evolution, ecosystem carbon storage, and ecological processes, playing pivotal roles [66,67]. The topographic position index (TPI) integrates elevation and slope derivatives from DEMs to quantitatively delineate landform morphology, effectively reflecting the integrated impacts of terrain on spatial heterogeneity [68]. TPI values exhibit a positive correlation with fluctuations in elevation and slope. Higher TPI values indicate more pronounced transitions from low-lying areas to highlands, representing a wide range of terrain including plains, gentle slopes, steep slopes, and mountain ridges. Conversely, smaller TPI values correspond to relatively depressed landforms such as valleys and basins. The computational formula for TPI is as follows:

$$T = In[(E/E_0 + 1) \times (S/S_0 + 1)] \quad (14)$$

where T represents the topographic position index; E, $\bar{E}_0$, S, S_0 denote the elevation (m), average elevation (m), slope (°), and average slope (°) of each grid cell in the study region, respectively. The 5 natural breaks classification method was employed to categorize elevation, slope, and topographic position index into 5 classes in ascending order of their numeric values, namely I, II, III, IV, and V, as shown in Table 5.

Table 5. Classification criteria of elevation, slope, and topographic index for the Daiyun Mountain's Rim.

Classification	Elevation/m	Slope/(°)	Topographic Position Index
I	0–307	0–9.56	0–0.3
II	307–536	9.56–16.63	0.3–0.48
III	536–742	16.63–23.70	0.48–0.61
IV	742–990	23.70–32.08	0.61–0.74
V	990–1833	32.08–73.84	0.74–1.22

2.8. Optimal Parameter Geographic Detector (OPGD)

2.8.1. Parameter Optimization

The geographic detector is a novel tool for measuring, mining, and exploiting spatial geographic heterogeneity [69]. This study draws on relevant studies [70], discretizing the study area into 8 spatial grid scales: 0.5 km, 1 km, 1.5 km, 2 km, 2.5 km, 3 km, 3.5 km, and 4 km.

The parameter optimization process involves two key steps, spatial discretization optimization and spatial scale optimization, aiming to determine the optimal scale for spatial heterogeneity. Consequently, this study employed the R language, utilizing equal interval classification, natural breaks classification, quantile classification, geometric interval classification, and standard deviation classification, with the number of classes set from 3 to 9, and screening the combination with the highest q-value using the OPGD model. Finally, the 90th percentile of q-values for all driving factors was compared across the 8 spatial scales, and the scale corresponding to the highest percentile value was identified as the optimal spatial grid scale, best revealing the characteristics of spatial heterogeneity [53].

2.8.2. Geodetector

Based on the determination of the optimal spatial scale, we employed factor detection and interaction detection analysis to evaluate the explanatory power of the independent

and interactive effects of multiple factors on carbon storage changes. The calculation formula [71] is as follows:

$$q = 1 - \frac{1}{N\sigma^2}\sum_{i=1}^{L} N_i\sigma_i^2 \quad (15)$$

where N and N_i represent the number of units in the entire region and i stratum, respectively; L represents the independent variable's stratification. The q-value ranges from 0 to 1, with higher values indicating a greater influence of the factor on carbon storage changes.

3. Results

3.1. Land-Use Change

The land-use spatial patterns across the study area exhibit distinct spatial heterogeneity, as depicted in Figure 2 and Table 6. Forest land remains the dominant land cover, encompassing the largest area and displaying a wide distribution, accounting for over 88% of the entire area. From 1992 to 2022, fluctuations were observed in forest land area dynamics, with the most significant reduction reaching 41,890.14 hm^2; this reduction in forest land area was mainly in Yuxi, Yongtai, Daitian, and Dehua Counties. However, cultivated land and construction land areas demonstrated an expanding trend. Cultivated land constituted over 7% of the total area and experienced an overall expansion of 27,152.1 hm^2 between 1992 and 2022, primarily concentrated in the southeastern regions, low-elevation areas, and on both banks of the river. Additionally, the largest expansion areas in cultivated land were still in the four Counties of Youxi, Yongtai, Daitian, and Dehua. Cultivated land as a proportion of the total area experienced a decline during the period from 1992 to 2012, followed by a rapid expansion between 2017 and 2022. Construction land area overall increased by 13,612.41 hm^2, exhibiting a distinct expansionary trend; this was primarily concentrated near residential areas and cultivated lands, with Xianyou County experiencing the largest increase. Construction land area increased the most from 2012 to 2017, with an increase of 3447.27 hm^2, primarily originating from urban expansion, manifesting as a reduction in forest and cultivated land area coupled with an expansion in construction land area. Shrub, grassland, water bodies, and barren land constituted relatively small proportions of the total area and had sporadic patchy distributions, each representing less than 1% of the entire area. Water bodies primarily comprised larger lakes and rivers.

Table 6. Changes in land-use types in the Daiyun Mountain's Rim from 1992 to 2032 (hm^2).

Year	Cropland	Forest	Shrub	Grassland	Water Bodies	Barren	Impervious
1992	108,270.09	1,220,328.18	219.42	281.79	3207.33	0.18	3493.35
1997	104,427.72	1,222,148.52	252.99	194.31	3582.36	0.09	5194.35
2002	114,892.47	1,209,449.25	312.75	204.30	3713.67	0.09	7227.81
2007	104,654.79	1,217,775.78	275.94	288.36	4083.21	0.36	8721.90
2012	99,680.13	1,219,302.81	192.24	377.91	4590.72	4.14	11,652.39
2017	122,465.34	1,192,885.20	155.52	406.44	4777.83	10.35	15,099.66
2022	135,422.19	1,178,438.04	136.80	280.89	4402.98	13.68	17,105.76
2032 (ND)	165,165.57	1,142,040.69	681.39	276.84	4381.02	12.42	23,242.41
2032 (ED)	118,143.54	1,183,781.97	87.93	280.89	4933.71	4.14	28,568.16
2032 (EP)	99,829.8	1,213,293.96	87.93	221.49	5256.54	4.86	17,105.76
2032 (CD)	99,829.8	1,201,772.16	87.93	280.89	5257.26	4.14	28,568.16

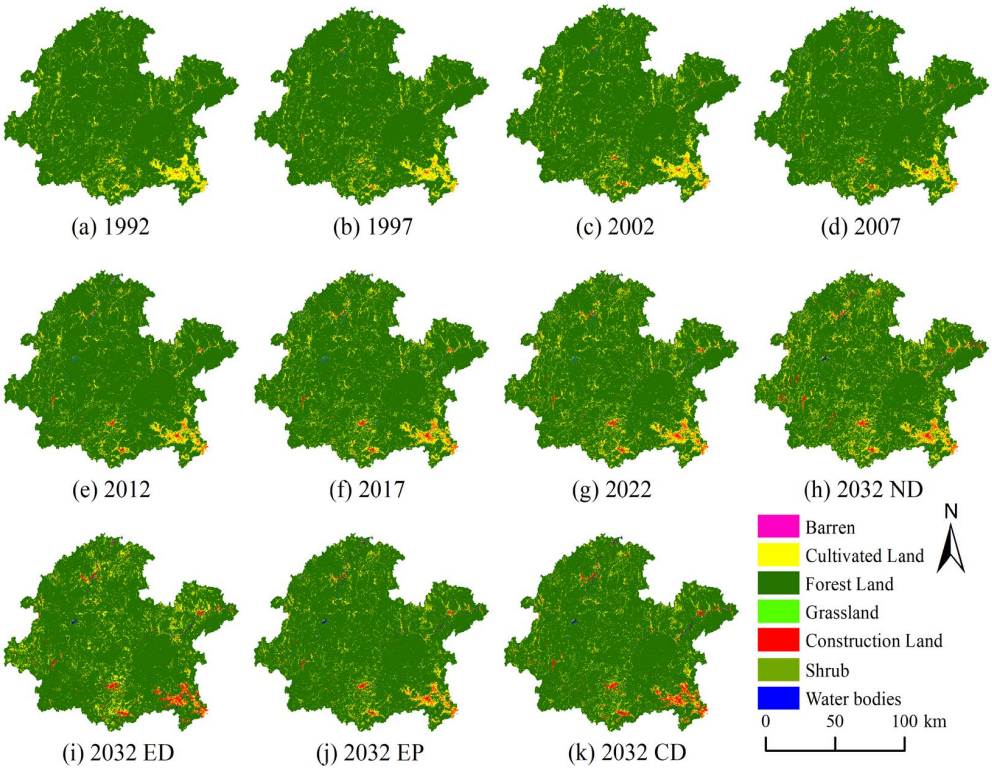

Figure 2. Spatial distribution characteristics of land-use types in the Daiyun Mountain's Rim from 1992 to 2032: (**a**–**g**) represent the spatial distribution of land-use types in 1992, 1997, 2002, 2007, 2012, 2017, and 2022 in the Daiyun Mountain's Rim, respectively; (**h**–**k**) represent the 2032 nature development scenario, 2032 economic priority development scenario, 2032 ecological priority development scenario, and 2032 coordinated economic and ecological development scenario in the Daiyun Mountain's Rim, respectively.

The simulated land-use results for 2032 (Figure 2) reveal disparities in area across different land-use types under varying scenarios compared to 2022. In the ND scenario, cultivated, shrub, and construction land areas expand significantly, increasing by 29,743.38 hm^2, 544.59 hm^2, and 6136.65 hm^2, respectively. The newly added cultivated land was adjacent to existing cultivated land, whereas the construction land that was newly added primarily concentrated near rivers. Other land-use types experienced area reductions, with forest land exhibiting a notable decrease of 36,397.35 hm^2. Under the ED scenario, cultivated, shrub, and barren land area decreased by 17,278.65 hm^2, 48.87 hm^2, and 9.54 hm^2, respectively, while construction land, forest land, and water bodies areas increased by 11,462.40 hm^2, 5343.93 hm^2, and 530.73 hm^2, respectively, with construction land area in Xianyou County expanding significantly. In the EP scenario, forest land and water bodies area increased by 34,855.92 hm^2 and 853.56 hm^2, respectively, whereas cultivated land area decreased by 35,592.39 hm^2. The newly added forest land was scattered, failing to form a clear aggregation area. Under the CD scenario, cultivated, shrub, and barren land area decreased by 35,592.39 hm^2, 48.87 hm^2, and 9.54 hm^2, respectively, while forest, water bodies, and construction land areas increased by 23,334.12 hm^2, 854.28 hm^2, and 11,462.40 hm^2, respectively.

3.2. Carbon Storage

Over the past 30 years, the ecosystem's carbon stocks of the Daiyun Mountain's Rim have exhibited a fluctuating trend characterized by growth and decline (Table 7). The cumulative carbon stocks decreased by 3.3 Tg, with the capacity to sequester carbon lowered by 2%, while the regional average carbon density remained within the range of

122.24–124.8 t·hm^{-2}. In terms of the different stages, the regional carbon stocks showed different characteristics before and after 2012. Between 1992 and 2012, the regional ecosystem's carbon stocks remained relatively stable, with a cumulative decrease of 0.17 Tg, a 0.1% decline, primarily due to the decrease in cultivated land area. However, the regional carbon stocks experienced a dramatic change from 2012 to 2022, with a significant decrease of 3.14 Tg and a 1.9% reduction, mainly attributable to the decline in forest land carbon stocks. Thus, it is evident that in the past decade, the carbon sink function of the Daiyun Mountain's Rim has accelerated in its decay rate.

Table 7. Carbon stock changes in various land-use types in the Daiyun Mountain's Rim from 1992 to 2032 (Tg).

Year	Cropland	Forest	Shrub	Grassland	Water Bodies	Barren	Impervious	Total
1992	6.04	160.20	0.01	0.02	0.15	0.00	0.16	166.59
1997	5.83	160.44	0.02	0.01	0.16	0.00	0.24	166.70
2002	6.41	158.78	0.02	0.01	0.17	0.00	0.34	165.72
2007	5.84	159.87	0.02	0.02	0.19	0.00	0.40	166.33
2012	5.56	160.07	0.01	0.02	0.21	0.00	0.54	166.42
2017	6.83	156.60	0.01	0.02	0.22	0.00	0.70	164.39
2022	7.56	154.71	0.01	0.02	0.20	0.00	0.79	163.28
2032 (ND)	9.22	149.93	0.04	0.02	0.20	0.00	1.08	160.48
2032 (ED)	6.59	155.41	0.01	0.02	0.22	0.00	1.33	163.57
2032 (EP)	5.57	159.28	0.01	0.01	0.24	0.00	0.79	165.90
2032 (CD)	5.57	157.77	0.01	0.02	0.24	0.00	1.33	164.93

Compared to the carbon stocks in 2022, the natural development scenario in 2032 was reduced by 2.8 Tg, and the economic priority development scenario, ecological priority development scenario, and coordinated economic–ecological development scenario added 0.29 Tg, 2.62 Tg, and 1.65 Tg, respectively. In terms of the carbon stock changes across different land-use types, forest land carbon stocks increased, contrasting with the decrease in cultivated land carbon stocks under all scenarios except the natural development scenario. Under the policy requirements for ecological conservation, the total carbon stocks in the economic priority development scenario, ecological priority development scenario, and coordinated economic–ecological development scenario all experienced an increase, while cultivated land carbon stocks remained at a comparatively low level. This indicates that the coordinated growth of economy and ecology in the Daiyun Mountain's Rim is essentially a matter of allocating the areas of cultivated land and forest land. By reasonably adjusting the proportional areas of these two land-use types, a balance between economic growth and ecological conservation can be achieved.

From the spatial distribution perspective (Figure 3), the high-value carbon stock areas in the Daiyun Mountain's Rim are primarily located in the mountainous regions. This is strongly connected to the natural conditions of the Daiyun Mountains being a national nature reserve, dominated by forest vegetation, with abundant sunshine and rainfall, located in a subtropical monsoon climate region. The low-value carbon storage areas are scattered, mainly composed of cultivated land and construction land, with the largest low-value area in the southeast. The spatial distribution characteristics of carbon stock changes vary across different time scales. From 1992 to 2022, the areas of carbon storage increase and decrease exhibited a scattered distribution pattern within the six time periods, while over the entire 1992–2022 period, the changes in carbon storage showed a noticeable clustering effect. Under the economic priority development scenario, the spatial distribution of areas with increasing and decreasing carbon stocks are intertwined, appearing more concentrated

compared to the other three scenarios. In the natural development scenario, the areas with changes in carbon storage are primarily dominated by decreasing carbon storage regions. In the ecological priority development scenario, carbon stock changes are mainly characterized by increasing carbon storage areas. Under the coordinated economic and ecological development scenario, the areas of increasing carbon stocks are also relatively scattered, while the areas with decreasing carbon stocks are primarily clustered in the southeastern direction.

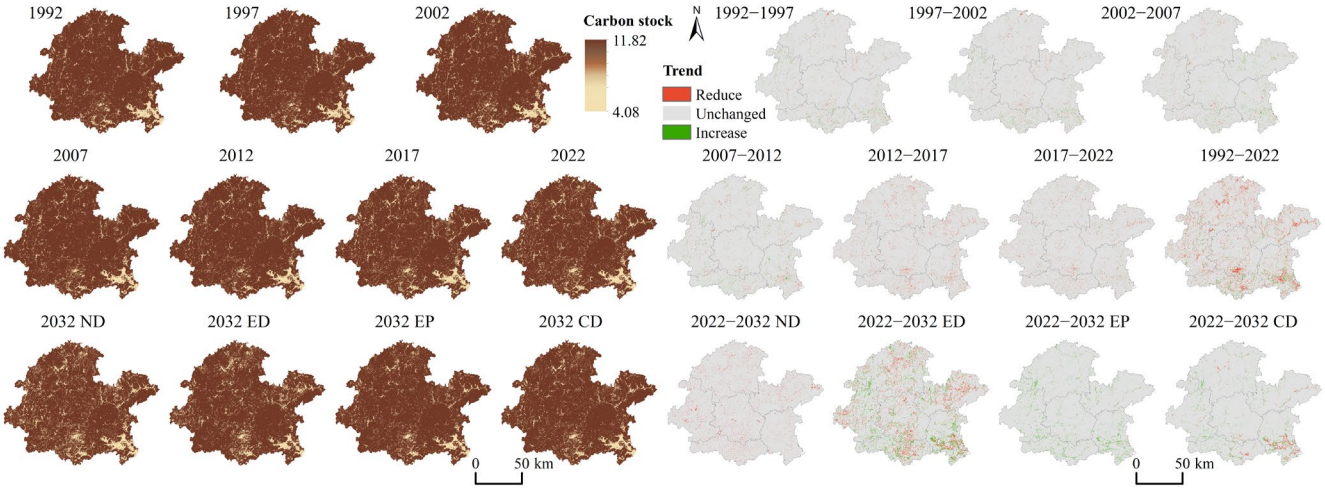

Figure 3. The spatial distribution pattern and change trend of carbon storage in the Daiyun Mountain's Rim from 1992 to 2032.

3.3. Influence of Land-Use Type Transfers on Carbon Storage Changes

The changes in carbon stocks were primarily influenced by conversion areas of land-use types and differences in carbon densities across land types. As shown in Figures 4 and 5, over the past 30 years, the land-use type conversions in the six counties of the Daiyun Mountain's Rim generally exhibited a trend of transitioning from high-carbon-density land types to low-carbon-density land types. The most active land conversions involved forest, cultivated, and construction land. Forest land area decreased by 41,890.14 hm^2, representing the largest transfer out of land type. Conversely, cultivated and construction land areas increased by 27,152.1 hm^2 and 13,612.41 hm^2, respectively, exhibiting a significant increase. Additionally, areas of water bodies and barren land also increased, while shrub and grassland areas slightly decreased. The aforementioned changes in land-use types accounted for approximately 7.2% of the total area, resulting in a carbon stock increase of 1.57 Tg and a decrease of 4.87 Tg, with a net decrease of 3.3 Tg. In terms of land-use type conversions that enhanced carbon sequestration capacity, cultivated land transfer to forest land increased carbon storage the most, representing this land conversion type with the highest carbon sequestration, reaching 1.53 Tg, followed by water bodies, shrubland, and grassland transfer to forest land. In terms of land-type conversions that weakened carbon sequestration capacity, forest land transfer to cultivated land was the primary reason for the decrease in carbon storage, amounting to 4.42 Tg, a reduction of nearly 2.66%. Furthermore, due to the demand for land by urbanization, a certain scale of forest land and cultivated land was transferred to construction land, resulting in significant carbon storage decreases of 0.3 Tg and 0.1 Tg, respectively. Other land-type conversions had minimal impact on carbon storage changes. It is evident that during the process of forest land area contraction, the reduction in carbon stocks far exceeded the increase in carbon stocks from the conversion of other land types to forest land, ultimately leading to an overall decrease

in carbon stocks in the Daiyun Mountain's Rim from 1992 to 2022. Forest, cultivated, and construction land are the three main land types influencing changes in carbon storage.

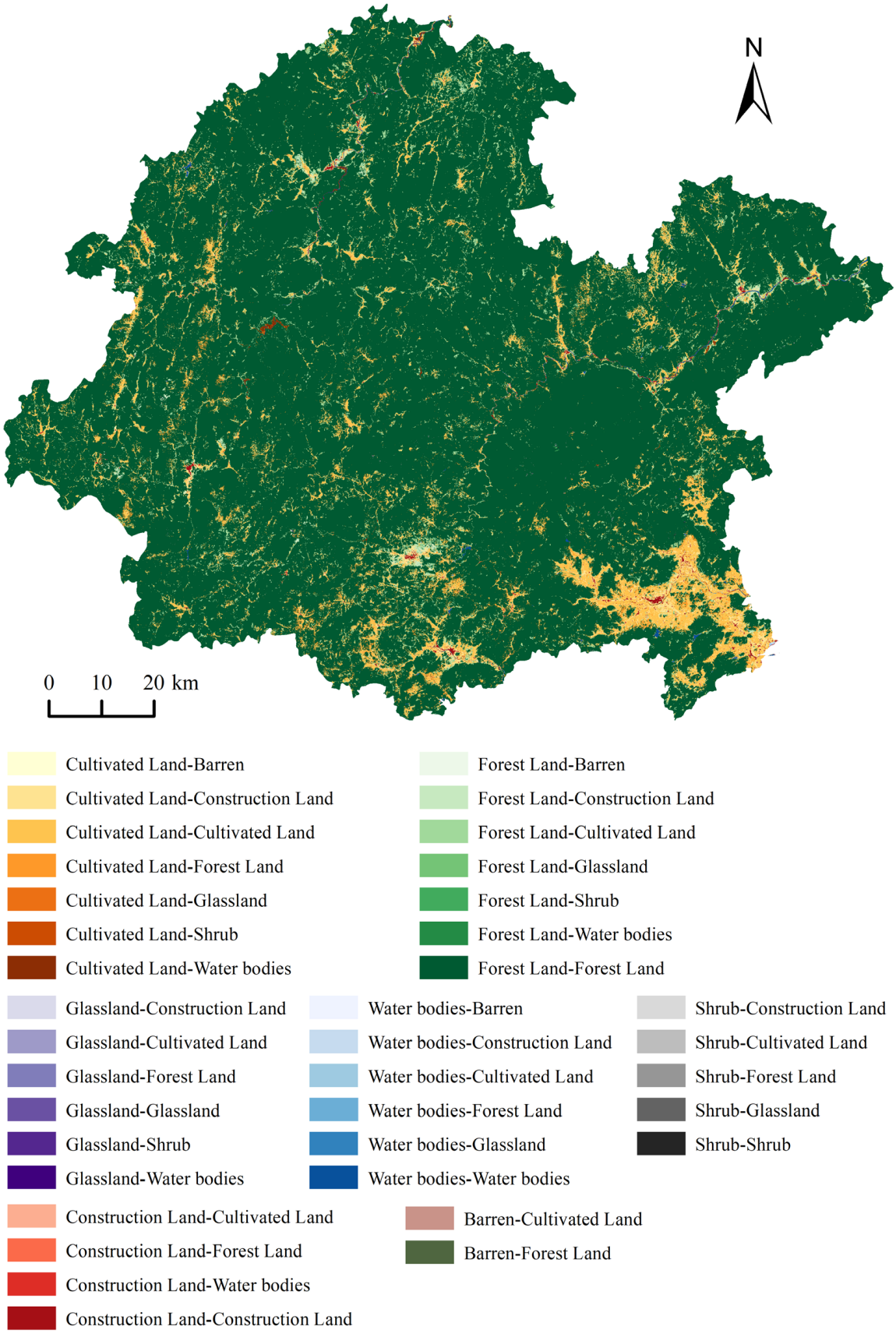

Figure 4. Spatial changes in land use in the Daiyun Mountain's Rim from 1992 to 2022.

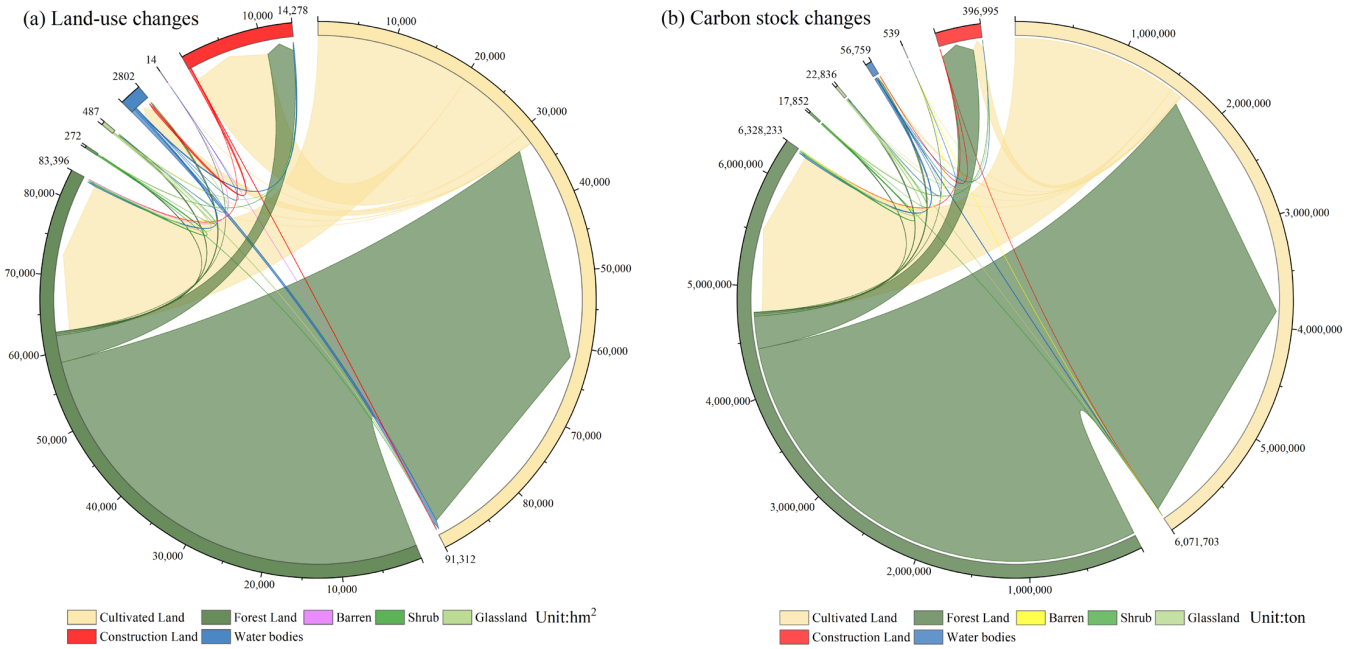

Figure 5. Changes in land uses and carbon stocks in the Daiyun Mountain's Rim from 1992 to 2022: (**a**) changes in land uses in the Daiyun Mountain's Rim from 1992 to 2022; (**b**) changes in carbon stocks in the Daiyun Mountain's Rim from 1992 to 2022.

From a county-level analysis (Figure 6), the six counties in the Daiyun Mountain's Rim exhibited varying degrees of spatial land conversion characteristics from 1992 to 2022. These included the transfer of cultivated land to forest land—which increased carbon sequestration capacity—as well as the transfer of forest land to cultivated and construction land and cultivated land to construction land, which decreased carbon sequestration capacity. Among these, the two most prominent were the increase in carbon stocks by transferring cultivated land to forest land and the decrease in carbon stocks by transferring forest land to cultivated land. Youxi County experienced the largest decrease in carbon storage, reaching 1.28 Tg. Within this county, carbon storage reduction from the transfer of forest land to cultivated land was the highest among the six counties, amounting to a staggering 1.32 Tg, while the increase in carbon stocks from the conversion of cultivated land to forest land was the lowest, at a mere 0.14 Tg. Conversely, Xianyou County witnessed the largest increase in carbon stocks from the transfer of cultivated land to forest land among the six counties, reaching 0.41 Tg, while the decrease in carbon stocks from forest land transfer to cultivated land was the smallest, at 0.5 Tg.

3.4. Topographic Distribution Patterns of Carbon Storage

The topography of the six counties of the Daiyun Mountain's Rim shows a high–low undulating distribution from northwest to southeast, overall presenting a landscape pattern of alternating high mountains and low valleys (Figure 1). From the distribution of carbon storage grades (Figure 7), 85% of the carbon stocks are concentrated in grades II-V. This is mainly because a large amount of forest land is distributed in this grade region. Only 7% of the forest land above 1000 m (grade V) is distributed in this region; therefore, grade V has the least carbon stocks, consistent with the result proposed by Xu et al. [68]. Additionally, shrubs and grasslands mainly distributed in grades III–V also increase the carbon storage capacity of high-altitude areas to some degree. From the viewpoint of slope grades, carbon stocks are mainly distributed in grades II–V; this aligns with the findings of Zhao et al. [72]. Carbon stocks first increase and then decrease as the slope grade increases. This may be the result of two factors: first, the steeper the slope, the richer the forest land vegetation

and the less human activity; second, there is a smaller area of grade V [68]. In addition, shrubs mainly distributed in the region of grade II–V slopes also increase carbon stocks in this grade region. Combined with the terrain index derived from elevation and slope parameters, it can intuitively reflect the distribution pattern of different land-use types. The topographic position index of the study region ranges from 0 to 1.22. The terrain undulation in the southeast region and river banks of the Daiyun Mountain's Rim (terrain index 0–0.48) is small, with a large amount of cultivated land distributed, as well as water systems and construction land. The carbon stocks are relatively low in this terrain index range, and the carbon storage shows an increasing trend as the terrain index increases. The terrain of most areas of the Daiyun Mountain's Rim is quite steep with great surface undulation (terrain index 0.48–0.74). The area of forest land and shrubs has greatly increased in this region, and carbon storage shows an increasing trend. Grade V (terrain index 0.74–1.22) has less carbon storage, which may be linked to its small area and less forest land area. As the terrain index increases, the average carbon storage shows an increasing trend.

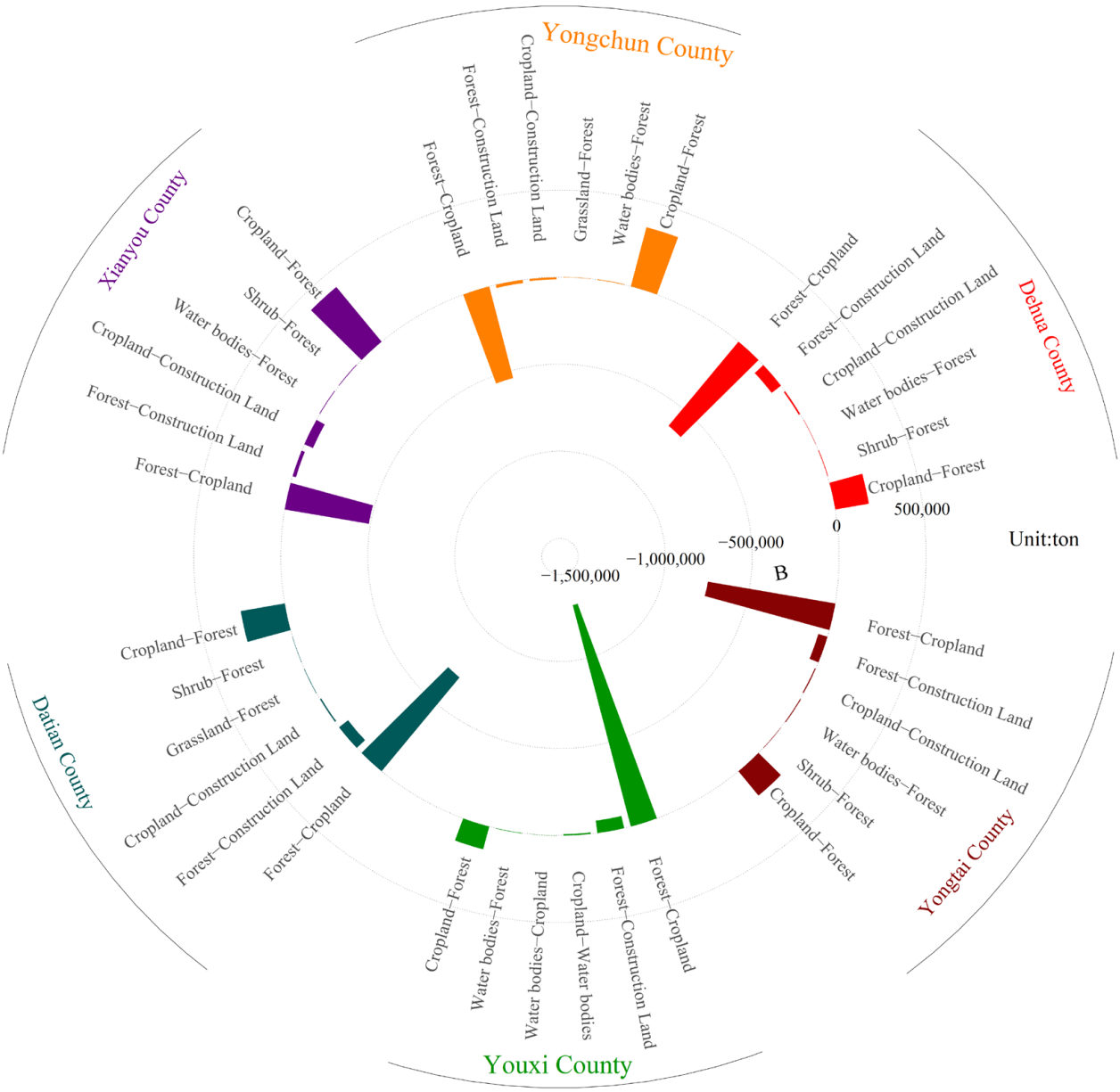

Figure 6. Impacts of major land type shifts on carbon stocks in different counties of the Daiyun Mountain's Rim.

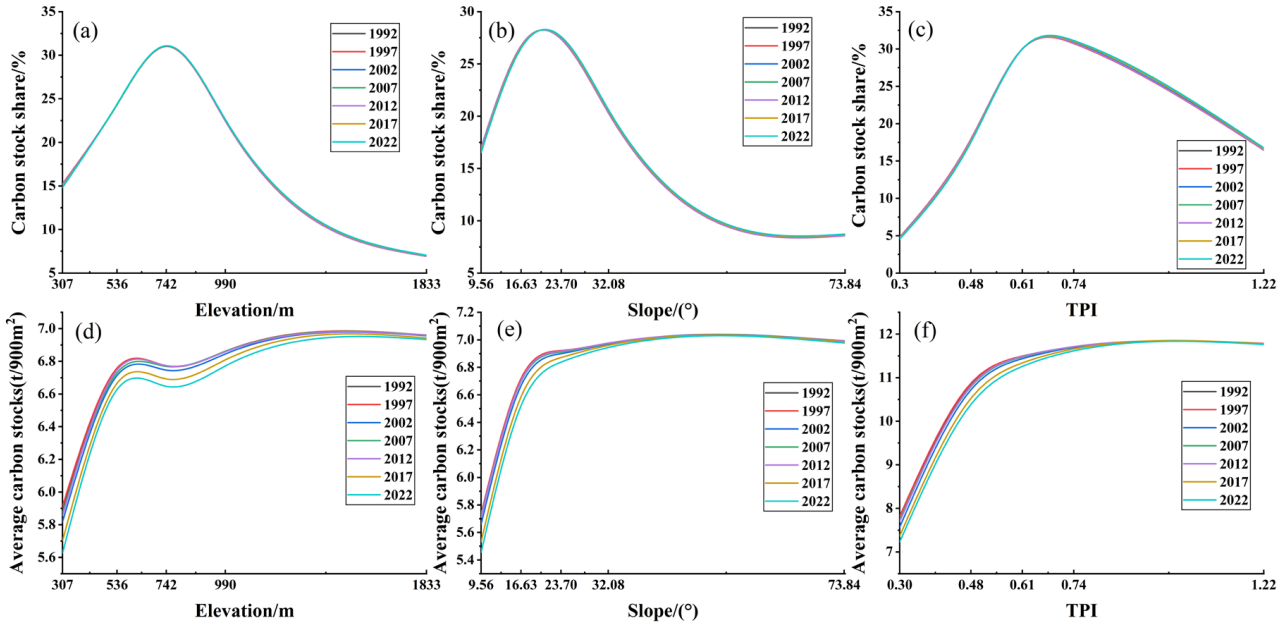

Figure 7. Distributional differentiation of carbon stocks in multi-dimensional topographic environments: (**a**) carbon storage changes at different elevations; (**b**) carbon storage changes across slope gradients; (**c**) carbon storage changes across topographic wetness index categories; (**d**) average carbon storage changes at different elevations; (**e**) average carbon storage changes across slope gradients; (**f**) average carbon storage changes across topographic wetness index categories.

3.5. Carbon Stock Driving Mechanisms

3.5.1. Optimal Parameter Identification

The analysis of eight different spatial grid scales reveals differences in the degree of influence exerted by the driving factors on carbon stocks within the study region (Table 8). As the spatial grid scale increases, most driving factors' explanatory power exhibit an upward trend, with some factors reaching their peak at a scale of 3.5 km. By ranking the q-values of all driving elements in descending order and selecting the 90th percentile, it is observed that this percentile value initially rises and then declines, reaching a maximum of 0.621 at the 3.5 km grid scale. This finding suggests that, compared to other spatial scales, adopting a 3.5 km grid scale more accurately reflects the degree of influence exerted by the various driving factors on the distribution of carbon stocks within the study area. Consequently, when exploring the spatial heterogeneity of carbon stocks and their underlying causes in this region, choosing 3.5 km as the optimal spatial scale will aid in obtaining more reasonable explanations. This spatial scale has the potential to reveal the dominant driving forces influencing the distribution of carbon storage to the greatest extent, thereby providing a deeper comprehension of the formation mechanism of spatial heterogeneity.

3.5.2. Driving Detection Analysis

1. Factor analysis

Through the implementation of a parameter-optimized geographical detector model, a single-factor exploration was conducted to assess the explanatory power of various individual driving factors on carbon stocks' spatial distribution characteristics in the Daiyun Mountain's Rim from 1992 to 2022 (Table 9). The results reveal that the annual mean temperature (0.6309) and night light index (0.6072) exhibited the strongest explanatory power for the spatial heterogeneity of carbon storage, with average q-values significantly higher than those of other driving factors, rendering them as key driving factors. Elevation (0.5282), slope (0.5033), and population density (0.4049) exhibited average q-values at a medium–high level, classifying them as major driving factors. Annual precipitation, gross

domestic product (GDP), distances to county and township government seats, soil type, and distances to secondary roads and primary roads had average q-values ranging from 0.1 to 0.3, categorizing them as secondary driving factors. Other driving factors demonstrated weaker interpretive potential for the spatial heterogeneity of carbon stocks, including distances to tertiary roads, distances to highways, vegetation net primary productivity, soil erosion intensity, aspect, distances to water bodies, and distances to quaternary roads [50].

Table 8. Comparison of 90% quartiles of q-values for factors at different spatial scales.

Factors	0.5 km	1 km	1.5 km	2 km	2.5 km	3 km	3.5 km	4 km
X1	0.3519	0.4238	0.4755	0.4729	0.5257	0.5142	0.5377	0.5143
X2	0.5483	0.5935	0.6023	0.5961	0.5705	0.5557	0.5047	0.5319
X3	0.0400	0.0392	0.0412	0.0387	0.0337	0.0471	0.0464	0.0222
X4	0.0995	0.1489	0.1770	0.2066	0.2282	0.2307	0.2791	0.2757
X5	0.3014	0.4060	0.4782	0.5154	0.5501	0.5696	0.6158	0.5889
X6	0.1494	0.1586	0.1906	0.1899	0.2035	0.2092	0.1939	0.2024
X7	0.0052	0.0090	0.0162	0.0195	0.0241	0.0462	0.0488	0.0585
X8	0.0738	0.0961	0.0971	0.1082	0.1096	0.1023	0.0551	0.1383
X9	0.0891	0.1215	0.1631	0.1652	0.1967	0.2004	0.2217	0.2493
X10	0.1531	0.2131	0.2903	0.3017	0.3123	0.3299	0.3587	0.1633
X11	0.3530	0.4679	0.5362	0.5694	0.6142	0.6056	0.6707	0.6616
X12	0.0320	0.0425	0.0523	0.0596	0.0662	0.0675	0.0920	0.0901
X13	0.0436	0.0657	0.0894	0.1061	0.1181	0.1268	0.1767	0.1675
X14	0.1157	0.1534	0.1761	0.1827	0.1909	0.1961	0.2030	0.2358
X15	0.0509	0.0624	0.0700	0.0709	0.0717	0.0932	0.0802	0.0796
X16	0.0267	0.0275	0.0271	0.0228	0.0226	0.0277	0.0160	0.0274
X17	0.0701	0.0678	0.0628	0.0545	0.0579	0.0612	0.0307	0.0403
X18	0.1173	0.1616	0.1928	0.2040	0.2113	0.2303	0.2235	0.2712
90% quartile	0.373	0.48	0.543	0.572	0.575	0.573	0.621	0.596

Table 9. Explanatory power (q) of the single factor for the spatial heterogeneity of carbon stocks in the Daiyun Mountain's Rim from 1992 to 2022.

Factors	1992	1997	2002	2007	2012	2017	2022	1992–2022
X1	0.5311	0.5347	0.5225	0.5153	0.5363	0.5196	0.5377	0.5282
X2	0.4996	0.5006	0.4984	0.4931	0.5015	0.5255	0.5047	0.5033
X3	0.0447	0.0474	0.0439	0.0452	0.0446	0.0448	0.0464	0.0453
X4	0.2849	0.2839	0.2701	0.2635	0.2765	0.2581	0.2791	0.2737
X5	0.6577	0.6559	0.6359	0.6230	0.6288	0.5991	0.6158	0.6309
X6	0.2137	0.2101	0.2154	0.2118	0.2100	0.2192	0.1939	0.2106
X7	0.0644	0.0675	0.0683	0.0561	0.0469	0.0436	0.0488	0.0565
X8	0.0593	0.0634	0.0616	0.0570	0.0548	0.0556	0.0551	0.0581
X9	0.2733	0.2600	0.2486	0.2449	0.2295	0.2182	0.2217	0.2423
X10	0.4423	0.4335	0.4215	0.4156	0.4010	0.3614	0.3587	0.4049
X11	0.5727	0.5820	0.5668	0.5885	0.6283	0.6413	0.6707	0.6072
X12	0.0671	0.0632	0.0661	0.0681	0.0730	0.0765	0.0920	0.0723
X13	0.1703	0.1749	0.1629	0.1514	0.1490	0.1457	0.1767	0.1615
X14	0.1732	0.1727	0.1628	0.1775	0.1930	0.1957	0.2030	0.1825
X15	0.0653	0.0665	0.0735	0.0769	0.0793	0.0822	0.0802	0.0748
X16	0.0259	0.0250	0.0261	0.0232	0.0244	0.0246	0.0160	0.0236
X17	0.0371	0.0369	0.0373	0.0416	0.0427	0.0424	0.0307	0.0384
X18	0.2132	0.2160	0.2200	0.2229	0.2254	0.2378	0.2235	0.2227

2. Interaction detection

The spatial distribution characteristics of carbon stocks are the outcome of complex interactions among multiple driving factors. An examination of the interactive detection results (Figure 8) reveals that the interaction among driving factors has a much stronger explanatory power than that of individual factors for the heterogeneity of carbon stock distribution within the research area. Notably, the explanatory power of the night light index as a single factor surpasses its interactive explanatory power with certain other factors. During the period from 2012 to 2022, the dominant factors influencing spatial heterogeneity in carbon storage exhibited significant interactive effects with other variables. The mean annual temperature demonstrated explanatory power ranging from 0.6504 to 0.6992, while the night light index showed values between 0.6089 and 0.6942. Elevation and slope gradients contributed with ranges of 0.6098–0.6321 and 0.6312–0.655, respectively, whereas population density exhibited interactions within 0.5077–0.5807. These parameters consistently emerged as the paramount interactive driving forces within the study region. Among these, the interaction between annual mean temperature and slope in the Daiyun Mountain's Rim exhibited the strongest explanatory power during 1992–2007, ranging from 0.7633 to 0.7905, while the interaction between night light index and slope had the strongest explanatory power during 2012–2022, ranging from 0.7935 to 0.8123, indicating that their interactions significantly influenced the formation of the spatial distribution pattern of carbon stocks. The q-value change from 1992 to 2022 reveals that the interactions of six driving factors—annual mean temperature, soil type, soil erosion intensity, vegetation net primary productivity, GDP, and population density—with other factors generally exhibited a weakening trend. Their average interactive explanatory power decreased by 0.0361, 0.0266, 0.0149, 0.0057, 0.0487, and 0.0736, respectively. In contrast, the night light index exhibited markedly strengthened interactions with other factors, achieving an increased explanatory power of 0.0706. The interactions among locational factors overall exhibited a slightly increasing trend. This suggests that socioeconomic factors, represented by the night light index, exerted a substantial influence on carbon storage and this influence became increasingly significant. Natural factors dominated the impact on carbon storage but their influence declined. Locational factors had the weakest impact on carbon storage but their influence slightly increased.

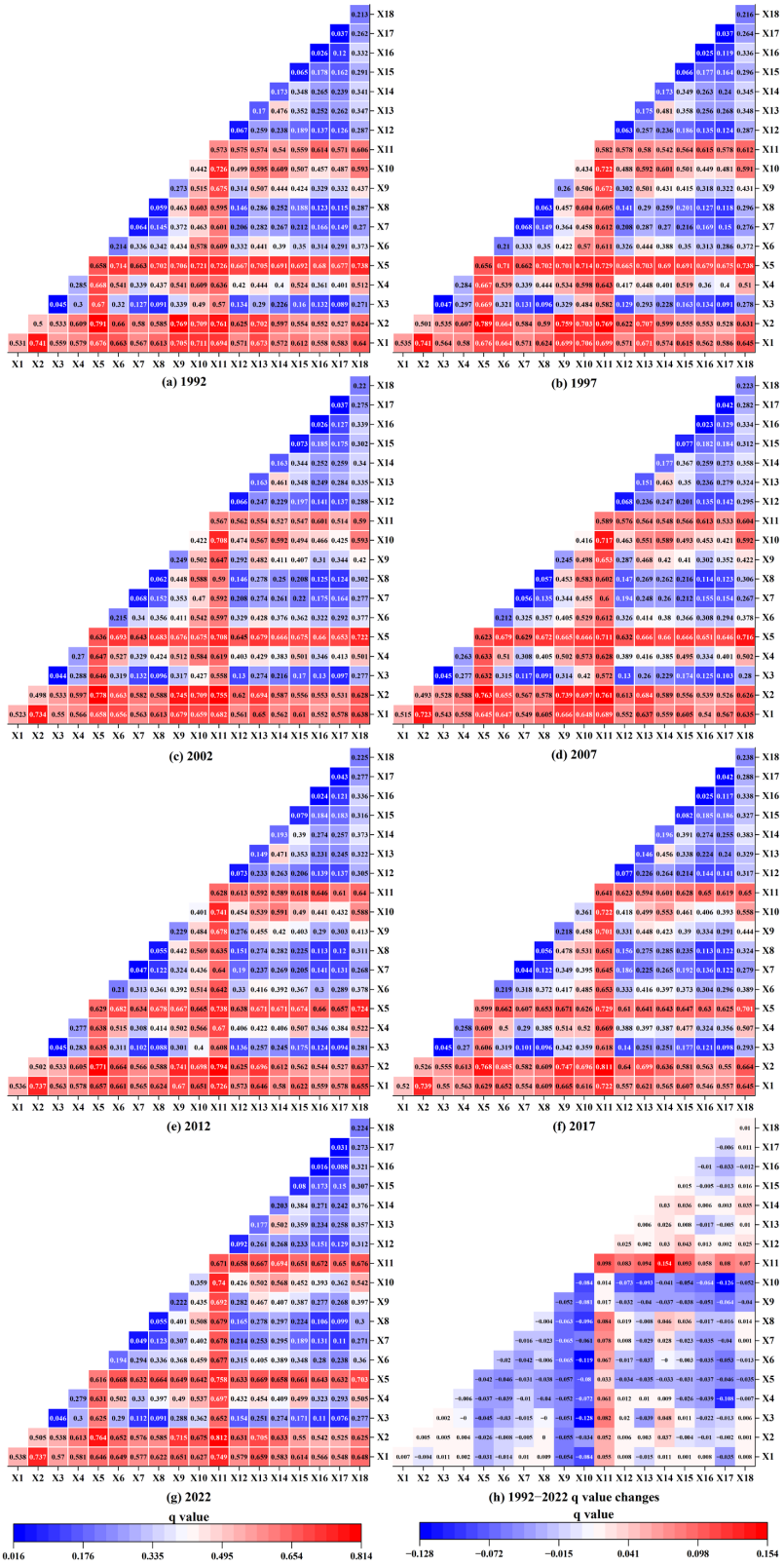

Figure 8. Results of the interactive detection of carbon stock drivers in the Daiyun Mountain's Rim from 1992 to 2002: (**a**–**g**) represent the results of the interactive detection of carbon stock drivers in 1992, 1997, 2002, 2007, 2012, 2017, and 2022 in the Daiyun Mountain's Rim, respectively, and the legend is below figure (**g**); (**h**) represent the value changes in the Daiyun Mountain's Rim from 1992 to 2022, and the legend is below figure (**h**).

4. Discussion

4.1. Feasibility Analysis of Carbon Storage Estimation

The accuracy of the carbon density data used in the InVEST model to estimate carbon stocks determines the accuracy of the carbon stocks estimation results. The data used for carbon density calculation in this paper mainly come from the World Soil database and the corresponding parameters of the National Ecological Science Data Center. In comparison with the relevant literature, Tong et al. [73] summarized the research results of land-use data, soil carbon sink, and land-use management carbon sink, and concluded that the 1 m soil carbon density in Fujian Province in 2020 was 125.32 t·hm^{-2}. In contrast, this study's carbon density at 0.3 m for various land-use types ranges from 45.23 to 51.05 t·hm^{-2}, which is higher than the previous results but the difference is not large. The primary reason is that the forest vegetation coverage in the study area is high and the biodiversity is rich, resulting in higher soil carbon density than the average level in Fujian Province. Based on the soil organic carbon data obtained from a multi-objective regional geochemical survey, Wang [74] calculated the average carbon density of 0.2 m soil organic carbon in Fujian Province as 34.45 t·hm^{-2} using the method of unit soil carbon amount. The average carbon density of soil organic carbon of different land-use types ranges from 29.84 to 36.54 t·hm^{-2}, which is very close to this study's carbon density at 0.3 m of various land-use types ranging from 45.23 to 51.05 t·hm^{-2}. Zeng et al. [75] sampled the topsoil of residential land in Nantai Island, Fuzhou City, and measured the topsoil organic carbon density of residential land as 43.48 t·hm^{-2}, which is also very close to the construction land's value of 45.23 t·hm^{-2} soil carbon density in this study. The comparative analysis with existing research results shows that the soil carbon density calculation method and the final carbon density values adopted in this paper are quite consistent with the results calculated based on measured data or official data, displaying the high accuracy of this method and its ability to depict carbon stock changes in the Daiyun Mountain's Rim.

4.2. Drivers of Spatiotemporal Patterns in Land-Use Change and Carbon Storage

Over the past 30 years, different land-use types and carbon stock changes in the Daiyun Mountain's Rim have shown dynamic fluctuations, mainly due to the joint influence of multiple factors such as agricultural policies, economic growth, and population migration. Han Y. et al. [65] found in their research that the increasing and then decreasing trend of carbon stocks in the Zhongtiao Mountain ecosystem in southern Shanxi from 2000 to 2016 may be related to ecological reconstruction projects and policies like the Grain for Green, which verifies the findings of this study. Specifically, the Grain for Green program and the diversification of rural livelihoods caused the area under cultivation to shrink and the area covered by forests to grow, and carbon sequestration increased slightly. From 1997 to 2002, the national government substantially increased agricultural investment, while Fujian Province simultaneously implemented a comprehensive land utilization plan (1997–2010), projecting an additional 72,000 hectares of cultivated land. During this period, agricultural activities dominated the rural economic structure [76], resulting in a resurgence of arable land area, a decline in forestland, and, consequently, a reduction in carbon storage capacity. During the 2002–2012 interval, the nationwide implementation of the first Grain-for-Green policy initiative prompted a significant exodus of rural labor. In Fujian Province, the collective forest rights system reform was instituted in 2003. The national government proposed the "West Coast Economic Zone" strategy in 2004 (elevated to national strategy status in 2009), followed by the formulation of the West Coast Urban Agglomeration Development Plan in 2010. Throughout this decade, under the accelerated urbanization and regional development framework centered on Xiamen–Zhangzhou–Quanzhou, cultivated land diminished substantially, while forestland

expanded rapidly, leading to a recovery in carbon storage. From 2012 to 2022, the national focus shifted predominantly toward ecological development. This period witnessed the implementation of agricultural supply-side reforms and rural revitalization policies. Fujian Province successively gained approval as an Ecological Civilization Pilot Demonstration Zone (2014) and National Ecological Civilization Experimental Zone (2016). Concurrently, several national initiatives bolstered Fujian's economic development, including the "China (Fujian) Pilot Free Trade Zone", the "21st Century Maritime Silk Road Core Area", the "Fuzhou New Area", and the "Fujian–Xiamen–Quanzhou National Independent Innovation Demonstration Zone". During this phase, cultivated land experienced renewed growth while forestland decreased, resulting in a decline in carbon storage capacity.

The areas of significant carbon stock changes in the Daiyun Mountain's Rim are concentrated in the intersection areas of forest, cultivated, and construction land. The main reason for this stems from the shift in cultivated and forest land to construction land in six counties, while the expansion of cultivated land is also largely a result of the reduction in forest land. Among them, in counties with less cultivated land and abundant forest resources—such as Yongchun County, Youxi County, and Dehua County—large tracts of forest land area were transferred to construction and cultivated land during economic development, incurring an immense ecological cost. In Xianyou County, where cultivated land resources are relatively abundant, the conversion mainly encroached upon the agricultural spaces surrounding urban areas and water bodies within cities. From 1992 to 2022, the area of forest land transferred to cultivated land reached as high as 586.23 hm^2, resulting in the greatest loss of carbon stocks of 4.424 Tg. Forest land transferred to cultivated land was the predominant type of land-use change during this period, also driving carbon stock changes in the region. The carbon stock changes resulted from the aforementioned conversions among different land types, essentially reflecting the interplay among forest, cultivated, and construction land utilization. This fully demonstrates that human activities have profoundly influenced the spatial distribution pattern of carbon stocks in the Daiyun Mountain's Rim. Rational planning of cultivated and forest land is of paramount importance for existing policy guidelines.

The GMOP-PLUS model employed in this study can more effectively resolve the quantitative and spatial conflicts among different land-use types, achieving an approximate optimal solution for the objective [77] while also adhering more closely to objective reality. Compared to 2022, the carbon storage projections for all three scenarios (economic priority development scenario, ecological priority development scenario, and coordinated economic–ecological development scenario) in 2032 exhibited a certain increase, whereas the carbon stock loss under the natural development scenario exceeds the carbon stock gains across other scenarios, indicating that the natural development scenario is inadvisable. The cultivated land area decreased in all three scenarios, reflecting the inevitable trend of decreasing cultivated land area under the dual context of economic growth and ecological environmental conservation. In the ecological priority development scenario, projections for 2032 indicate that construction land area would remain stagnant compared to 2022 levels, revealing a significant disparity with actual regional development requirements, thus rendering this scenario less viable. While both the coordinated economic–ecological development and economic priority development scenarios maximize construction land area while maintaining minimum arable land requirements, the former demonstrates notable advantages in carbon storage capacity. Given Fujian Province's strategic positioning as a national ecological civilization pilot zone, the economic–ecological synergistic development scenario better aligns with future regional development needs, emerging as the optimal developmental pathway. According to scholarly research, increasing the planting density of advantageous tree species, thereby increasing the carbon density of forest land,

is an effective pathway to enhance regional carbon storage [41]. Concurrently, this study also argues that through crop rotation, improving crop yields per unit area, and straw mulching techniques, not only can these increase the economic output efficiency of farmed land but they also enable the full utilization of light and temperature resources, thereby increasing the carbon storage of cultivated land. Furthermore, elevating the spatial resource utilization rate and economic output efficiency per unit area of construction land will help to curb the disorderly expansion of this land. The above measures aim to promote intensive and efficient land utilization, providing an effective way to resolve the land-use conflicts between economic growth and ecological civilization construction.

This study identified two key driving factors and three major driving factors affecting carbon stocks in the Daiyun Mountain's Rim during various periods, with the single-factor exploration and their interaction with other factors exhibiting the strongest explanatory power for carbon storage, indicating that the effects of the factors affecting carbon stocks in this region were generally stable. However, the factor combination with the strongest explanatory power in the interaction exploration shifted from slope and mean annual temperature to slope and night light index, reflecting that although natural factors maintain a dominant influence on carbon storage, their impact is declining, while the influence of socioeconomic factors is markedly increasing. This further substantiates the deepening impact of human activities on regional carbon stocks. The root cause lies in human's ability to adapt to and exploit nature, overcoming limitations posed by slope, temperature, and other natural environmental constraints, leading to the utilization of more land and, consequently, reducing regional carbon stocks. In the context of regional carbon stock management, the impact of human activities must be highly prioritized, and corresponding measures should be adopted to mitigate their adverse effects on carbon storage.

4.3. Suggestions for Ecosystem Synergy and Co-Benefits

Terrestrial ecosystems are sensitive and fragile, vulnerable to both natural and anthropogenic disturbances [78]. How to keep terrestrial ecosystems stable and orderly while enhancing their carbon fixation ability is an urgent problem to be solved under the background of ecological space compression in the Daiyun Mountain's Rim and similar areas in Southern China. The research findings indicate that interactions among various driving factors can intensify their impact on the spatial heterogeneity of carbon stocks, necessitating fully utilizing the synergistic effects between various driving factors. For instance, based on the findings that regions with high topographic indices, such as high altitude and high slope, have strong carbon sequestration capabilities, future efforts in the Daiyun Mountain's Rim should focus on implementing and consolidating vegetation protection and increasing vegetation planting density in areas with high topographic indices—particularly mountainous regions above 300 m in elevation—to prevent forest land transfer to other land-use types. However, the preceding analysis focuses on ecological impacts, and human needs must also be considered. Economic growth follows the optimal allocation law of scarce resources across different competitive purposes [79], while ecosystem products—such as regulating ecosystem products (such as climate regulation, water conservation, etc.) and cultural ecosystem products (such as recreation, aesthetic value, etc.) [80]—inherently lack exclusivity and scarcity unless exploited. In 2022, General Secretary Xi Jinping emphasized that forest lands are reservoirs, banks, granaries, and carbon sinks. Accordingly, by granting market scarcity to ecological products through technical means or other innovative forms, transforming them into people's income, and transforming the competitive relationship between humans and ecosystems into a collaborative one, this is an important path to balance economic growth and ecological environmental preservation in the Daiyun Mountain's Rim. For instance, bolstering the bamboo industry in Jian'ou and Yong'an Counties,

Fujian could raise bamboo farmers' incomes [81]. In addition, future research could focus on cultivating understory agriculture and pursuing adaptive and regional research and study activities with biodiversity as the theme. These are all important measures to realize the value of ecological goods. Given this, the regional green economic industry alliance in the Daiyun Mountain's Rim should manage and operate the terrestrial ecosystem in the Daiyun Mountain's Rim based on ecological environmental protection, effective utilization of ecological resources, enabling socio-ecological synergy, mutual benefit, and win–win results, supporting the realization of "dual carbon" goals to combat climate change.

4.4. Limitations and Future Enhancements

This study calculated soil carbon density using its own research area of soil data, which better reflects the actual conditions of the study area compared to most studies that cite previous research results. Although soil organic carbon has stability, soil organic carbon density changes with climate and environmental changes. However, due to data limitations and the enormous sampling workload, the carbon density data used in this study are not the carbon density data for each year during the study period; therefore, there is some loss of accuracy in estimating annual carbon storage, and future research should focus on exploring carbon density of different land-use types over the years. Secondly, this study mostly used spatial data, with resolutions of 30–1000 m, and higher resolution data could be used in the future.

The study area encompassed six county-level administrative units, representing a relatively small scale. Future research could expand to provincial or national scales. While this study employed the PLUS model, which is suitable for small-scale analyses, CLUMondo is more appropriate for larger-scale studies. CLUMondo demonstrates superior applicability in predicting ecosystem service multi-functionality under various future scenarios as it represents an enhanced iteration of the CLUE model. Its distinctive feature lies in incorporating land system changes driven by goods and services demand, while comprehensively accounting for human activity intensity and socioeconomic development impacts on land-use patterns.

Considering that PLUS is predominantly utilized by Chinese researchers while CLUMondo is more prevalent internationally, and given China's unique developmental context of balancing economic growth with environmental protection, this study established four future development scenarios. Moving forward, the selection between PLUS and CLUMondo models should be guided by study area scale and regional characteristics, with scenarios tailored to local development trajectories.

5. Conclusions

Based on seven periods of land-use data from 1992 to 2022, along with natural factor data, socioeconomic data, and accessibility data, this study used an integrated GMOP, PLUS, InVEST, and OPGD modeling approach to simulate carbon storage under multiple scenarios in the Daiyun Mountain's Rim for 2032, which better aligns with regional policy planning and actual conditions. Based on the 30-year-long time-series data, the model systematically analyzed the characteristics and spatial heterogeneity of land-use and carbon storage changes in this region, introducing a terrain position index perspective to deepen the understanding of carbon storage spatial distribution patterns, and detected the driving mechanisms of carbon storage changes from multiple dimensions of natural–socioeconomic–road accessibility factors. The conclusions are as follows:

(1) Vegetation cover in the Daiyun Mountain's Rim is predominantly forest land, followed by cultivated and construction land. From 1992 to 2022, forest land area in the region decreased significantly by 41,890.14 hm^2, while cultivated and construction land

areas increased by 27,152.1 hm^2 and 13,612.41 hm^2, respectively. In 2032, under the natural development scenario, forest land area will continue to decrease significantly, while the areas of cultivated, shrub, and construction land will further expand. However, under the economic priority development scenario, ecological priority development scenario, and economic–ecological coordinated development scenario, cultivated land area will exhibit a declining trend;

(2) From 1992 to 2022, the region's carbon stocks displayed a fluctuating trend of increase and decrease, with a cumulative decrease of 3.3 Tg. The average carbon storage ranged from 122.24 to 124.8 $t \cdot hm^{-2}$ and the rate of carbon storage decrease accelerated in the last 10 years. Youxi County experienced the largest decrease in carbon storage, while Xianyou County generated the greatest amount of carbon stocks from cultivated land transferred to forest land. Carbon storage initially increased and then decreased with increasing altitude, slope, and terrain position index, exhibiting a decreasing trend after the turning points of 742 m altitude, 23.7° slope, and 0.74 terrain position index. The average carbon storage increased with increasing altitude, slope, and terrain position index. Compared to 2022, carbon storage in 2032 will decrease by 2.8 Tg under the natural development scenario but increase by 0.29 Tg, 2.62 Tg, and 1.65 Tg under the economic priority development, ecological priority development, and economic–ecological coordinated development scenarios, respectively. The spatial distribution of carbon stock variations in the region exhibits a scattered pattern;

(3) Land-use changes in the region and its six counties mainly manifested as mutual conversions among forest, cultivated, and construction land, with forest land transferred to cultivated land being the primary type and dominant type of carbon storage change. Overall, approximately 7.2% of the land-use types underwent conversion, with forest land being the primary outgoing land type and cultivated and construction land being the primary incoming land type;

(4) The key factors influencing carbon storage in the region are mean annual temperature and night light index, with the major driving factors being elevation, slope, and population density. There are six secondary driving factors and seven other factors. Multi-factor interactions have significantly higher explanatory power for carbon storage heterogeneity than individual factors, with the interactions between mean annual temperature, night light index, elevation, slope, population density, and other factors being the most important interactive dominant factors. The effect of natural factors on carbon stocks is declining, while the influence of socioeconomic factors is rising.

In summary, the ecosystem carbon stocks in the Daiyun Mountain's Rim experienced an overall decline from 2019 to 2022, mainly influenced by agricultural policies, economic development, and population mobility. To enhance regional carbon storage, a balance should be sought between ecological protection and economic development, and the following measures are proposed: First, precautions should be used to protect and manage vegetation in the Daiyun Mountain's Rim, particularly the vegetation at high altitudes and on steep slopes. Second, the utilization rate of light and temperature resources in cultivated land, as well as the planting density of advantageous tree species, should be improved. Third, the scarcity of ecological products in the region should be enhanced through technological means or other innovative forms, promoting the sharing of benefits between the ecosystem and human society. This will not only avoid competition between the two but also create economic value for incentive protection. This approach will not only increase regional carbon storage but also provide support for achieving the "dual carbon" goals and addressing climate change, offering a valuable reference for sustainable development and ecological environment protection decision-making in the hilly areas of Southern China.

Supplementary Materials: The following supporting information can be downloaded at: https://www.mdpi.com/article/10.3390/land14010014/s1.

Author Contributions: Conceptualization, G.C. and K.S.; methodology, G.C. and Q.F.; software, G.C. and Q.F.; validation, G.C., W.L. and K.S.; formal analysis, G.C. and Q.P.; investigation, G.C., W.L. and K.S.; writing—original draft preparation, G.C. and Q.P.; writing—review and editing, W.L. and K.S.; supervision, W.L. and K.S.; funding acquisition, W.L. and K.S. All authors have read and agreed to the published version of the manuscript.

Funding: This research was funded by the Humanity and Social Science Foundation of the Ministry of Education of China (Grant No. 23YJCZH192), the Major Project Funding for the Social Science Research Base in Fujian Province Social Science Planning: Ecological Civilization Research Center (Grant No. FJ2022JDZ035), the Science and Technology Innovation Special Fund Project of Fujian Agriculture and Forestry University (Grant No. CXZX2020037A), and the National Scientific Research Project Cultivation Plan of Anxi College of Tea Science of Fujian Agricultural and Forestry University (Grant No ACKY2023011). The authors also thank "Fujian–Taiwan Joint Innovative Centre for Germplasm Resources and Cultivation of Crop (Grant No. 2015-75)" for their support.

Data Availability Statement: The original contributions presented in this study are included in the Supplementary Materials. Further inquiries can be directed to the corresponding author.

Conflicts of Interest: The authors declare no conflicts of interest.

References

1. Hodson, R. Climate Change. *Nature* **2017**, *550*, S53. [CrossRef]
2. Xu, L.; Yu, G.; He, N.; Wang, Q.; Gao, Y.; Wen, D.; Li, S.; Niu, S.; Ge, J. Carbon Storage in China's Terrestrial Ecosystems: A Synthesis. *Sci. Rep.* **2018**, *8*, 2806. [CrossRef] [PubMed]
3. Hu, Y.; Li, Y.; Zhang, H.; Liu, X.; Zheng, Y.; Gong, H. The Trajectory of Carbon Emissions and Terrestrial Carbon Sinks at the Provincial Level in China. *Sci. Rep.* **2024**, *14*, 5828. [CrossRef]
4. Paruke, W.; Ai, D.; Ji, Z.X.; Duan, W.K.; Wang, N.; Hao, J.M. The spatial transition of "production-living-ecological" space in Beijing and its effect on carbon storage under the perspective of human-land relation. *China Environ. Sci.* **2023**, *44*, 1–17. [CrossRef]
5. Malik, A.A.; Puissant, J.; Buckeridge, K.M.; Goodall, T.; Jehmlich, N.; Chowdhury, S.; Gweon, H.S.; Peyton, J.M.; Mason, K.E.; van Agtmaal, M.; et al. Land Use Driven Change in Soil pH Affects Microbial Carbon Cycling Processes. *Nat. Commun.* **2018**, *9*, 3591. [CrossRef] [PubMed]
6. Popp, A.; Calvin, K.; Fujimori, S.; Havlik, P.; Humpenöder, F.; Stehfest, E.; Bodirsky, B.L.; Dietrich, J.P.; Doelmann, J.C.; Gusti, M.; et al. Land-Use Futures in the Shared Socio-Economic Pathways. *Glob. Environ. Chang.* **2017**, *42*, 331–345. [CrossRef]
7. Song, X.P.; Hansen, M.C.; Stehman, S.V.; Potapov, P.V.; Tyukavina, A.; Vermote, E.F.; Townshend, J.R. Global Land Change from 1982 to 2016. *Nature* **2018**, *560*, 639–643. [CrossRef]
8. Su, K.; Wei, D.Z.; Lin, W.X. Evaluation of Ecosystem Services Value and Its Implications for Policy Making in China—A Case Study of Fujian Province. *Ecol. Indic.* **2020**, *108*, 105752. [CrossRef]
9. Arneth, A.; Sitch, S.; Pongratz, J.; Stocker, B.D.; Ciais, P.; Poulter, B.; Bayer, A.D.; Bondeau, A.; Calle, L.; Chini, L.P.; et al. Historical Carbon Dioxide Emissions Caused by Land-Use Changes Are Possibly Larger than Assumed. *Nat. Geosci.* **2017**, *10*, 79–84. [CrossRef]
10. Solomon, S. IPCC (2007): Climate Change The Physical Science Basis. *Am. Geophys. Union* **2007**, *9*, 123–124.
11. Fu, Y.; He, Y.; Chen, W.; Xiao, W.; Ren, H.; Shi, Y.; Hu, Z. Dynamics of Carbon Storage Driven by Land Use/Land Cover Transformation in Coal Mining Areas with a High Groundwater Table: A Case Study of Yanzhou Coal Mine, China. *Environ. Res.* **2024**, *247*, 118392. [CrossRef] [PubMed]
12. Kauppi, P.E.; Mielikäinen, K.; Kuusela, K. Biomass and Carbon Budget of European Forests, 1971 to 1990. *Science* **1992**, *256*, 70–74. [CrossRef] [PubMed]
13. Tans, P.P.; Fung, I.Y.; Takahashi, T. Observational Contrains on the Global Atmospheric CO_2 Budget. *Science* **1990**, *247*, 1431–1438. [CrossRef] [PubMed]
14. Harris, N.L.; Gibbs, D.A.; Baccini, A.; Birdsey, R.A.; de Bruin, S.; Farina, M.; Fatoyinbo, L.; Hansen, M.C.; Herold, M.; Houghton, R.A.; et al. Global Maps of Twenty-First Century Forest Carbon Fluxes. *Nat. Clim. Chang.* **2021**, *11*, 234–240. [CrossRef]
15. Hiraishi, T.; Krug, T.; Tanabe, K.; Srivastava, N.; Baasansuren, J.; Fukuda, M.; Troxler, T.G. *2013 Supplement to the 2006 IPCC Guidelines for National Greenhouse Gas Inventories: Wetlands*; IPCC: Geneva, Switzerland, 2014.

16. Hiraishi, T.; Krug, T.; Tanabe, K.; Srivastava, N.; Baasansuren, J.; Fukuda, M.; Troxler, T.G. *2013 Revised Supplementary Methods and Good Practice Guidance Arising from the Kyoto Protocol*; IPCC: Geneva, Switzerland, 2014.
17. United Nations Climate Change Conference UK Glasgow Leaders' Declaration on Forests and Land Use. Available online: https://casaclimate.org/glasgow-leaders-declaration-on-forests-and-land-use/ (accessed on 10 December 2024).
18. Xinhua China Maps Path to Carbon Peak, Neutrality Under New Development Philosophy. Available online: https://english.www.gov.cn/policies/latestreleases/202110/24/content_WS61755fe9c6d0df57f98e3bed.html (accessed on 23 December 2023).
19. Lin, S.; Yu, F.W.; Liu, Y.Q. Philosophical Foundation, Ecological Implication and Practice Promotion of the "Dual Carbon" Goal under Marxist Practice View. *Res. Econ. Manag.* **2023**, 142–155. [CrossRef]
20. Zhao, X.; Ma, X.W.; Chen, B.Y.; Shang, Y.P.; Song, M.L. Challenges toward Carbon Neutrality in China: Strategies and Countermeasures. *Resour. Conserv. Recycl.* **2022**, *176*, 105959. [CrossRef]
21. Lu, F.X.; Zhang, Y.; Qin, Y.C.; Chen, Z.L.; Wang, G.H. Spatial patterns of provincial carbon source and sink in China. *Prog. Geogr.* **2013**, *32*, 1751–1759. [CrossRef]
22. Zhao, M.M.; Zhao, N.; Liu, Y.; Liu, Y.; Yue, T.X. An overview of forest carbon measurement methods. *Acta Ecol. Sin.* **2019**, *39*, 3797–3807. [CrossRef]
23. Lipatov, D.N.; Shcheglov, A.I.; Manakhov, D.V.; Brekhov, P.T. Spatial Variation of Organic Carbon Stocks in Peat Soils and Gleyzems in the Northeast of Sakhalin Island. *Eurasian Soil Sci.* **2021**, *54*, 226–237. [CrossRef]
24. Xiao, J.; Chevallier, F.; Gomez, C.; Guanter, L.; Hicke, J.A.; Huete, A.R.; Ichii, K.; Ni, W.; Pang, Y.; Rahman, A.F.; et al. Remote Sensing of the Terrestrial Carbon Cycle: A Review of Advances over 50 Years. *Remote Sens. Environ.* **2019**, *233*, 111383. [CrossRef]
25. Wang, C.W.; Luo, J.J.; Tang, H.H. Analysis on the Driving Force of Spatial and Temporal Differentiation of Carbon Storage in the Taihang Mountains Based on InVEST Model. *Ecol. Environ.* **2023**, *32*, 10662. [CrossRef]
26. Lu, L.; Xue, Q.; Zhang, X.; Qin, C.; Jia, L. Spatiotemporal Variation and Quantitative Attribution of Carbon Storage Based on Multiple Satellite Data and a Coupled Model for Jinan City, China. *Remote Sens.* **2023**, *15*, 4472. [CrossRef]
27. Babbar, D.; Areendran, G.; Sahana, M.; Sarma, K.; Raj, K.; Sivadas, A. Assessment and Prediction of Carbon Sequestration Using Markov Chain and InVEST Model in Sariska Tiger Reserve, India. *J. Clean. Prod.* **2021**, *278*, 123333. [CrossRef]
28. Wei, Q.; Abudureheman, M.; Halike, A.; Yao, K.; Yao, L.; Tang, H.; Tuheti, B. Temporal and Spatial Variation Analysis of Habitat Quality on the PLUS-InVEST Model for Ebinur Lake Basin, China. *Ecol. Indic.* **2022**, *145*, 109632. [CrossRef]
29. Li, J.; Gong, J.; Guldmann, J.-M.; Li, S.; Zhu, J. Carbon Dynamics in the Northeastern Qinghai–Tibetan Plateau from 1990 to 2030 Using Landsat Land Use/Cover Change Data. *Remote Sens.* **2020**, *12*, 528. [CrossRef]
30. Bacani, V.M.; Machado da Silva, B.H.; Ayumi de Souza Amede Sato, A.; Souza Sampaio, B.D.; Rodrigues da Cunha, E.; Pereira Vick, E.; Ribeiro de Oliveira, V.F.; Decco, H.F. Carbon Storage and Sequestration in a Eucalyptus Productive Zone in the Brazilian Cerrado, Using the Ca-Markov/Random Forest and InVEST Models. *J. Clean. Prod.* **2024**, *444*, 141291. [CrossRef]
31. Yu, Z.L.; Zhao, M.S.; Gao, Y.F.; Wang, T.; Zhao, Z.D.; Wang, S. Multiscenario Simulation and Prediction of Land Use in Huaibei City Based on CLUE-S and PLUS Models. *Appl. Sci.* **2023**, *13*, 7142. [CrossRef]
32. Wang, Z.Y.; Li, X.; Mao, Y.T.; Li, L.; Wang, X.R.; Lin, Q. Dynamic Simulation of Land Use Change and Assessment of Carbon Storage Based on Climate Change Scenarios at the City Level: A Case Study of Bortala, China. *Ecol. Indic.* **2022**, *134*, 108499. [CrossRef]
33. Lyu, R.F.; Mi, L.N.; Zhang, J.M.; Xu, M.Q.; Li, J.J. Modeling the Effects of Urban Expansion on Regional Carbon Storage by Coupling SLEUTH-3r Model and InVEST Model. *Ecol. Res.* **2019**, *34*, 380–393. [CrossRef]
34. Xia, Q.S.; Hong, X.; Gui, X.; Shen, G.P.; Deng, L.; Yao, Z.H.; Peng, P.; Chu, Y.Z.; Xu, S.; Xu, W. A Study on Carbon Fixation Capacity and Its Influencing Factors Based on InVEST Model at Wuhu City. *Bull. Soil Water Conserv.* **2023**, *43*, 385–394. [CrossRef]
35. Zhang, G.L. Spatial Distribution Characteristics of Carbon Storage of Urban Forests in Shanghai Based on Remote Sensing Estimation. *Ecol. Environ.* **2021**, *30*, 1777–1786. [CrossRef]
36. Zou, T.H.; Chen, P.; Liu, J.F.; Du, H.S. Spatio-temporal dynamics of territorial ecosystem carbon storage under different land use scenarios in Siping City. *China Environ. Sci.* **2023**, *43*, 5508–5518. [CrossRef]
37. Liang, X.; Guan, Q.; Clarke, K.C.; Liu, S.; Wang, B.; Yao, Y. Understanding the Drivers of Sustainable Land Expansion Using a Patch-Generating Land Use Simulation (PLUS) Model: A Case Study in Wuhan, China. *Comput. Environ. Urban Syst.* **2021**, *85*, 101569. [CrossRef]
38. Li, X.; Fu, J.Y.; Jiang, D.; Lin, G.; Cao, C.L. Land Use Optimization in Ningbo City with a Coupled GA and PLUS Model. *J. Clean. Prod.* **2022**, *375*, 134004. [CrossRef]
39. Li, Y.H.; Yao, S.; Jiang, H.Z.; Wang, H.R.; Ran, Q.C.; Gao, X.Y.; Ding, X.Y.; Ge, D.D. Spatial-Temporal Evolution and Prediction of Carbon Storage: An Integrated Framework Based on the MOP–PLUS–InVEST Model and an Applied Case Study in Hangzhou, East China. *Land* **2022**, *11*, 2213. [CrossRef]
40. Huang, H.; Xue, J.; Feng, X.; Zhao, J.; Sun, H.; Hu, Y.; Ma, Y. Thriving Arid Oasis Urban Agglomerations: Optimizing Ecosystem Services Pattern under Future Climate Change Scenarios Using Dynamic Bayesian Network. *J. Environ. Manag.* **2024**, *350*, 119612. [CrossRef] [PubMed]

41. Huang, T. Evaluation of Land Use Change and Carbon Storage in Fujian Province Based on PLUS-InVEST Model. *J. Soil Water Conserv.* **2024**, *38*, 246–257. [CrossRef]
42. Yang, L.; Xie, Y.W.; Zong, L.L.; Qiu, T.; Jiao, J.Z. Land Use Optimization Configuration based on Multi-Objective Genetic Algorithm and FLUS Model of Agro-pastoral Ecotone in Northwest China. *J. Geo-Inf. Sci.* **2020**, *22*, 568–579. [CrossRef]
43. Ji, X.H.; Cao, Y.Q.; Yao, J.Q.; Zhai, H.R.; Fan, J. Land use and ecosystem carbon storage change and prediction in the Haihe River basin. *South-North Water Transf. Water Sci. Technol.* **2023**, *21*, 985–995. [CrossRef]
44. Jiang, C.; Chen, H. Multi-Scenario Simulation of Urban–Rural Land Use Spatial Reconstruction in Highly Urbanized Areas: A Case Study from the Southern Jiangsu Region. *Land.* **2024**, *13*, 2199. [CrossRef]
45. Liu, Y.; Jing, Y.; Han, S. Multi-Scenario Simulation of Land Use/Land Cover Change and Water Yield Evaluation Coupled with the GMOP-PLUS-InVEST Model: A Case Study of the Nansi Lake Basin in China. *Ecol. Indic.* **2023**, *155*, 110926. [CrossRef]
46. Wang, Z.Y.; Meng, L.; Li, L.; Fang, X.; Qing, L. Multi-scenario simulation of land use and ecosystem services in Beijing under the background of low-carbon development. *Acta Ecol. Sin.* **2023**, *43*, 3571–3581. [CrossRef]
47. Liang, X.; Liu, X.P.; Li, D.; Zhao, H.; Chen, G.Z. Urban Growth Simulation by Incorporating Planning Policies into a CA-Based Future Land-Use Simulation Model. *Int. J. Geogr. Inf. Sci.* **2018**, *32*, 2294–2316. [CrossRef]
48. Xu, J.; Liu, H. Assessment and prediction of ecosystem services and their trade-offs and synergies in Gansu Province based on the GMMOP-PLUS model. *China Environ. Sci.* **2023**, *11*, 1–15. [CrossRef]
49. Fu, K.X.; Jia, G.D.; Yu, X.X.; Chen, L.X. Analysis of Temporal and Spatial Carbon Stock Changes and Driving Mechanism in Xinjiang Region by Coupled PLUS-InVEST-Geodector Model. *Environ. Sci.* **2024**, *45*, 5416–5430. [CrossRef]
50. Mu, F.Y.; Huang, Q.; Chen, L. Eco-environmental Quality Driving Force Detection Using Optimized Geographic Detector. *Res. Soil Water Conserv.* **2024**, *31*, 440–449. [CrossRef]
51. Dai, E.F.; Wang, Y.H. Spatial heterogeneity and driving mechanisms of water yield service in the Hengduan Mountain region. *Acta Geogr. Sin.* **2020**, *75*, 607–619. [CrossRef]
52. Lü, W.B.; Xu, Z.J.; Qi, G.; Wang, J.J.; Li, Z. Research on the Temporal Evolution and Spatial Differentiation Characteristics of Carbon Storage in Terrestrial Ecosystems on the Loess Plateau. *Res. Soil Water Conserv.* **2024**, *31*, 252–263. [CrossRef]
53. Song, Y.Z.; Wang, J.F.; Ge, Y.; Xu, C.D. An Optimal Parameters-Based Geographical Detector Model Enhances Geographic Characteristics of Explanatory Variables for Spatial Heterogeneity Analysis: Cases with Different Types of Spatial Data. *GIScience Remote Sens.* **2020**, *57*, 593–610. [CrossRef]
54. Wang, L.J.; Ma, S.; Xu, J.C.; Zhu, D.Z.; Zhang, J.C. Selection of priority protected region based on ecosystem service trade-offs: A case study of the southern hill and mountain belt, China. *Acta Ecol. Sin.* **2021**, *41*, 1716–1727. [CrossRef]
55. Liang, M.X. The Ecosystem Service Valuation of Daiyunshan Nature Reserve in Fujian. *J. Northwest For. Univ.* **2014**, *29*, 263–268. [CrossRef]
56. Si, X.Q.; Wang, X.J.; Lin, Y.B.; Liu, G.X. Spatiotemporal Characteristics of Carbon Storage and Its Response to Land Use Change in Fujian Province. *Bull. Soil Water Conserv.* **2023**, *43*, 355–364. [CrossRef]
57. Wu, Z.Y.; Liu, X.G.; Zeng, J.F. Spatio-temporal change and prediction of carbon storage in Dongjiang River source watershed based on InVEST-PLUS model. *Acta Sci. Circumstantiae* **2024**, *44*, 419–430. [CrossRef]
58. Xing, X.C.; Zhi, L.; Xie, Y.M.; Yuan, Z. Estimation of Ecological Service Value in Western Natural Forest Protection Project Area Based on Equivalent Factor Approach of Unit Area Value:Taking Six Western Provinces as an Example. *Ecol. Econ.* **2017**, *33*, 195–199.
59. Xie, G.D.; Zhang, C.X.; Zhang, L.M.; Chen, W.H.; Li, S.M. Improvement of the Evaluation Method for Ecosystem Service Value Based on Per Unit Area. *J. Nat. Resour.* **2015**, *30*, 1243–1254. [CrossRef]
60. Wang, Y.; Li, X.M.; Zhang, Q.; Li, J.F.; Zhou, X.W. Projections of Future Land Use Changes: Multiple Scenarios-Based Impacts Analysis on Ecosystem Services for Wuhan City, China. *Ecol. Indic.* **2018**, *94*, 430–445. [CrossRef]
61. Moreira, M.; Fonseca, C.; Vergílio, M.; Calado, H.; Gil, A. Spatial Assessment of Habitat Conservation Status in a Macaronesian Island Based on the InVEST Model: A Case Study of Pico Island (Azores, Portugal). *Land Use Policy* **2018**, *78*, 637–649. [CrossRef]
62. Chen, X.; Yu, L.; Hou, S.; Liu, T.; Li, X.; Li, Y.; Du, Z.; Li, C.; Wu, H.; Gao, G.; et al. Unraveling Carbon Stock Dynamics and Their Determinants in China's Loess Plateau over the Past 40 Years. *Ecol. Indic.* **2024**, *159*, 111760. [CrossRef]
63. Wang, Y.; Meng, J.J.; Qi, Y.; Peng, F.L. Review of Ecosystem Management Based on the InVEST Model. *Chin. J. Ecol.* **2015**, *34*, 3526–3532. [CrossRef]
64. Wang, S.Q.; Zhou, C.H. Estimating soil carbon reservior of terrestrial ecosystem in China. *Geogr. Res.* **1999**, *18*, 349–356.
65. Han, Y.; Ding, S.T.; Yang, T.B. Spatial and temporal distribution and driving factors of carbon storage in Zhongtiao Mountain ecosystem in southern Shanxi Province. *China Environ. Sci.* **2023**, *43*, 1298–1306. [CrossRef]
66. Lyu, J.H.; Qiao, Y.; Wang, Y.; Lyu, X.Y. Analysis of Spatial Spillover Effect and Threshold Effect of Forest Carbon Stocks in China. *J. Agro-For. Econ. Manag.* **2023**, *23*, 1–14.
67. Mugagga, F.; Kakembo, V.; Buyinza, M. Land Use Changes on the Slopes of Mount Elgon and the Implications for the Occurrence of Landslides. *Catena* **2012**, *90*, 39–46. [CrossRef]

68. Xu, C.X.; Gong, J.; Li, Y.; Yan, L.L.; Gao, B.L. Spatial distribution characteristics of typical ecosystem services based on terrain gradients of Bailongjiang Watershed in Gansu. *Acta Ecol. Sin.* **2020**, *40*, 4291–4301. [CrossRef]
69. Wang, J.F.; Xu, C.D. Geodetector: Principle and prospective. *Acta Geogr. Sin.* **2017**, *72*, 116–134. [CrossRef]
70. Yang, K.; Xin, G.X.; Jiang, H.Y.; Yang, C.X. Study on Spatiotemporal Changes of Landscape Ecological Risk Based on the Optimal Spatial Scale: A Case Study of Jiangjin District, Chongqing City. *J. Ecol. Rural Environ.* **2021**, *37*, 576–586. [CrossRef]
71. Chen, S.; Liu, X.; Yang, L.; Zhu, Z. Variations in Ecosystem Service Value and Its Driving Factors in the Nanjing Metropolitan Area of China. *Forests* **2023**, *14*, 113. [CrossRef]
72. Zhao, F.Y.; Wang, Q.F.; Zhang, H.T.; Chen, Z.P.; Zhang, L. Temporal and Spatial Variations of Arbor Forest Carbon Storage of Gansu Province Based on InVEST Model in the Forest Area of the Qilian Mountains. *J. Northwest For. Univ.* **2023**, *38*, 233–240. [CrossRef]
73. Tong, R.X.; Liang, X.; Guan, Q.F.; Song, Y.; Chen, Y.L.; Wang, Q.Y.; Zheng, L.N.; Jin, Q.; Yu, Y.P.; He, J. Estimation of soil carbon storage change from land use and management at a high spatial resolution in China during 2000–2020. *Acta Geogr. Sin.* **2023**, *78*, 2209–2222. [CrossRef]
74. Wang, W.J. Reserve Estimation, Spatiotemporal Distribution and Its Influencing Factors of Soil Organic Carbon in Fujian Province, China. *Geoscience* **2019**, *33*, 1295. [CrossRef]
75. Zeng, H.D.; Xu, H.Q.; Liu, Z.C.; Huang, X.H.; Xiao, S.L. Variability of Soil Organic Carbon and Factors Affecting It in Residential Lands in a Rapidly Urbanizing Area: A Case Study of Nantai Island of Fuzhou City, China. *Acta Ecol. Sin.* **2018**, *38*, 1427–1435. [CrossRef]
76. Li, Y.S. On the change of reginal economic development pattern in Fujian province. *World Reg. Stud.* **2001**, *10*, 71–77.
77. Wang, Z.Y.; Zhang, J.Y.; Li, H.Y.; Su, W.C. Multi-scale spatio-temporal evolution and multi-scenario simulation of land use conflict in Chongqing. *Acta Ecol. Sin.* **2024**, *44*, 1024–1039. [CrossRef]
78. Chen, Y.; Li, X.; Min, M. Mapping for Terrestrial Ecosystem Services: A Review. In Proceedings of the 2019 8th International Conference on Agro-Geoinformatics (Agro-Geoinformatics), Istanbul, Turkey, 16–19 July 2019; pp. 1–6.
79. Daly, H.E.; Farley, J. *Ecological Economics, Second Edition: Principles and Applications*; Island Press: Washington, DC, USA, 2011; ISBN 978-1-59726-991-9.
80. Li, P.; Jiang, L.G.; Feng, Z.M.; Yu, X.B. Research progress on trade-offs and synergies of ecosystem services:an overview. *Acta Ecol. Sin.* **2012**, *32*, 5219–5229. [CrossRef]
81. Ma, Q.H.; Yang, Z. Cultivation Status of European Hazelnuts and Their Introducing Utilization in China. *J. Plant Genet. Resour.* **2022**, *24*, 599–614. [CrossRef]